CHAPTER ONE

Density functional theory for van der Waals complexes: Size matters

Montgomery Gray and John M. Herbert*
Department of Chemistry & Biochemistry, The Ohio State University, Columbus, OH, United States
*Corresponding author. e-mail address: herbert@chemistry.ohio-state.edu

Contents

Abstract

Over the past 25 years there has been remarkable progress towards accurate description of nonbonded interactions within the context of density functional theory (DFT). Various methods have been devised to capture London dispersion, which is the most exacting contribution to noncovalent interactions; these strategies include both new functionals as well as *ad hoc* dispersion corrections to existing functionals. At present, it is possible to compute interaction energies for small van der Waals complexes (containing ∼20 atoms) to an accuracy of ∼ 0.5 kcal/mol, using a range of dispersion-inclusive DFT methods that are reviewed here. Systematic tests reveal remarkable consistency across different methods, at least for small dimers. At the same time, the magnitude of the *ad hoc* dispersion corrections are systematically smaller than benchmark dispersion energies because some dispersion resides within

Annual Reports in Computational Chemistry, Volume 20
ISSN 1574-1400, https://doi.org/10.1016/bs.arcc.2024.03.001

the semilocal exchange-correlation functional, in a manner that is difficult to disentangle. Despite impressive results for small systems, the best contemporary DFT methods afford larger errors in systems with $\gtrsim$ 100 atoms, approaching 3–5 kcal/mol for total interaction energies, as compared to *ab initio* benchmarks, although the benchmarks themselves have larger uncertainties in systems of this size. Errors for larger systems vary widely from one DFT method to the next, with no discernible systematic trend. Nanoscale van der Waals complexes thus represent the new frontier in development of DFT for noncovalent interactions.

1. Overview of dispersion in DFT

Sanibel Symposia at the dawn of the 21st century were, in the hazy memory of one author, characterized by an obsession with potential energy curves for rare-gas dimers, computed using density functional theory (DFT) *(1–3)*. Already by 1995 there was evidence of problems for dispersion-bound systems *(4,5)* and a growing recognition of semilocal DFT's failure to describe long-range electron correlation and with it, dispersion interactions. This led to early efforts to describe dispersion using coupled Kohn-Sham response theory *(6–8)*, and to incorporate those ideas into an exchange-correlation (XC) functional that would be applicable to van der Waals (vdW) complexes *(9–15)*. (This history has been reviewed elsewhere *(16)*). These efforts would eventually bifurcate, with one coterie continuing the quest for a universal density functional to describe dispersion while others pursued near-term practical solutions based on *ad hoc* dispersion corrections to existing XC functionals. The former approach is exemplified by the so-called "van der Waals density functional" (vdW-DF) of Langreth and Lundqvist *(17–20)*, along with the simplified VV10 functional of Vydrov and Van Voorhis *(21–24)*. Each of these is a nonlocal correlation functional that contains the correct ingredients to describe long-range dispersion between non-overlapping charge densities. VV10 has since been incorporated into a new generation of XC functionals *(25–29)* that perform remarkably well for nonbonded interactions *(30)*.

An alternative to finding a universal density functional is to build a model for dispersion that can be incorporated into (or added onto) an existing XC functional *(31–34)*. Among these, Grimme's dispersion corrections have become ubiquitous *(34–37)*. In practice, these amount to atom–atom potentials of the form $-C_6/R^6$ and $-C_8/R^8$, along with three-body (triatom) corrections *(36–38)*, added to a semilocal or hybrid functional in the spirit of much earlier "Hartree-Fock plus dispersion" methods

(39–43). Short-range damping functions forestall any catastrophes as $R \to 0$ and also mitigate potential double-counting of electron correlation in regions of space where the monomer densities still overlap *(34)*. In this dispersion-corrected "DFT+D" approach, the double-counting issue has important ramifications for how the +D correction should be interpreted. This is a main point of discussion in the present chapter.

Other dispersion corrections use the self-consistent field (SCF) electron density to obtain *in situ* ("atoms-in-molecules") C_6, C_8, … coefficients that reflect the manner in which an atom is both confined and polarized by its environment *(31,32)*. The exchange dipole moment (XDM) model of Becke and Johnson is one such approach *(44–50)*, as is the Tkatchenko-Scheffler (TS) model *(51)*, sometimes called "vdW-TS" *(52)*. Both methods incorporate what Dobson has dubbed "type A" dispersion nonadditivity *(53)*, meaning that free-atom C_n coefficients are modified by the molecular environment. Separate from that effect, Dobson designates "type B" nonadditivity to reflect the fact that atom–atom dispersion interactions are screened by the presence of polarizable centers on other atoms *(53)*. These effects become larger with molecular size, leading to a breakdown in the pairwise atom–atom approximation *(54–56)*. To correct for this, explicit three-body dispersion corrections can be added, typically of the Axilrod-Teller-Muto (ATM) "triple-dipole" variety *(38,54–57)*, which is the leading three-body dispersion correction from third-order perturbation theory *(58,59)*. Alternatively, implicit nonadditivity can be incorporated by means of a density-dependent many-body dispersion (MBD) model, as pioneered by Tkatchenko and co-workers *(60–63)*. For density-based dispersion corrections, it is important to choose a (mostly) dispersion-free XC functional, lest there be substantial double-counting *(64)*, and to balance the range of the semilocal functional against that of the dispersion correction *(65)*.

The culmination of sundry efforts to incorporate dispersion into DFT can be seen in (Fig. 1) for two archetypal dispersion-bound systems, namely, a rare-gas dimer (Kr_2) and the face-to-face or "sandwich" configuration of $(C_6H_6)_2$, which is a typical example of a π-stacking interaction *(67–70)*. Figure 1A juxtaposes potential energy curves for the latter, computed using a variety of dispersion corrections applied to the Perdew-Burke-Ernzerhof (PBE) functional *(71)*, a semilocal generalized gradient approximation (GGA). In the absence of any *ad hoc* dispersion correction, this functional affords a potential energy profile that is strictly repulsive, and in that way it is representative of the early 21st-century state of affairs with

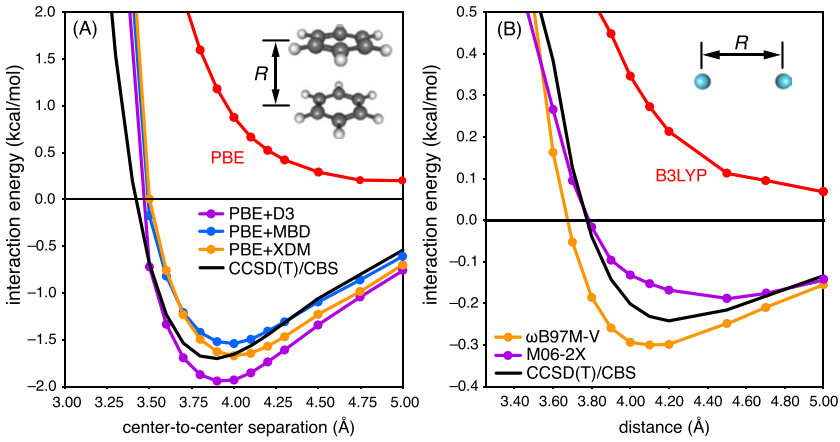

Fig. 1 Potential energy curves for dispersion-bound systems: (A) face-to-face "sandwich" configuration of benzene dimer in its D_{6h} geometry, and (B) krypton dimer. All DFT calculations use the def2-QZVPD basis set. CCSD(T)/CBS benchmarks for $(C_6H_6)_2$ are taken from Ref. *(66)*.

regard to nonbonded interactions in DFT. Addition of various dispersion corrections affords a reasonably accurate potential energy curve, as compared to a benchmark calculation at the CCSD(T) level *(66)*. (For a recent review of *ab initio* benchmarks for noncovalent systems, see Patkowski *(72)*). Interaction energies for the benzene dimer obtained using these dispersion-corrected PBE methods (PBE+D3, PBE+MBD, and PBE +XDM) lie in the range 1.5–1.9 kcal/mol, as compared to a complete basis-set (CBS) CCSD(T) benchmark value of 1.7 kcal/mol *(66)*. Equilibrium separations (in the D_{6h} geometry) range from 3.9–4.0 Å for dispersion-corrected PBE methods, as compared to the CCSD(T)/CBS value of 3.9 Å.

Hybrid DFT results for Kr_2 are presented in Fig. 1B. The B3LYP functional *(73,74)* affords an unbound potential curve, whereas results obtained using either M06-2X *(75)* or ωB97M-V *(26)* are reasonably accurate. Both of these functionals are meta-GGAs, according to the classification scheme known as Jacob's Ladder *(76–78)*, and are examples of methods designed to capture dispersion from first principles. Both functionals work rather well for this example, despite its extremely small interaction energy.

Together, these results are emblematic of the fact that in 2023, thirty years after hybrid functionals were shown to afford thermochemical

accuracies good enough to make chemists notice DFT *(73,79–82)*, noncovalent interactions now seem to have similarly been brought into the fold. Total interaction energies for small vdW complexes *(83–89)*, and relative conformational energies for larger organic molecules *(90–92)*, can now be predicted within $\lesssim$1 kcal/mol of benchmark values, using a variety of DFT-based strategies *(31,32)*. Geometries for small noncovalent dimers are also predicted accurately *(93)*. That said, for the dispersion-dominated interactions that are characteristic of small nonpolar molecules, the total interaction energy may itself be $\lesssim$1 kcal/mol. Perhaps it is simply the case that DFT cannot meaningfully distinguish these weakest interactions from zero, although the data for Kr_2 (Fig. 1B) provide reason for optimism. There, the benchmark interaction energy is smaller than 0.3 kcal/mol yet the best-performing functionals yield qualitatively correct potential energy profiles and total interaction energies $|E_{int}| = 0.2–0.3$ kcal/mol.

To determine whether statistically encouraging DFT results in small-dimer data sets are somehow a fluke, it is necessary to extend these benchmarks to much larger systems where even dispersion-dominated interaction energies greatly exceed 1 kcal/mol. For vdW complexes with $\gtrsim$100 atoms, dispersion interactions alone may exceed 50 kcal/mol in magnitude in some cases *(94,95)*. Meanwhile, the role of dispersion in predicting conformational energies of bonded molecular systems is better recognized now than it was three decades ago *(31,90–92,96,97)*, to the point where it is clear that dispersion forces cannot be ignored by the practicing organic chemist, as they may compete with steric repulsion and other nonbonded forces *(98–101,102,103)*. Dispersion forces are also critically important in liquids *(104–107,108,109)* and solids *(52,110–116)*.

Nevertheless, most benchmarking of dispersion-inclusive DFT methods has been limited to small nonbonded dimers. The uracil dimer, along with hydrocarbons up to pentane dimer, represent some of the larger systems in standard data sets *(72,117–126)*, for which reliable CCSD(T)/CBS benchmarks are available without additional approximations. There are a few larger *ab initio* benchmarks *(127–134)*, as surveyed recently *(130)*, and DFT results for some of these larger systems will be scrutinized herein. Meanwhile gas-phase experiments, based on cryogenic ion vibrational predissociation spectroscopy *(135)*, suggest that small-dimer benchmarks may not provide a representative picture of the situation in systems with $\gtrsim$150 atoms *(136–138)*. At the same time, most experimental binding affinities for noncovalent complexes are measured in solution, and although these have occasionally been used as benchmark tests for quantum

chemistry *(55,56,94,139–143)*, the largest source of uncertainty is the solvation correction *(139–141)*. Solution-phase benchmarks thus make for less incisive tests of how well dispersion is described by DFT, and will not be considered here.

The present chapter summarizes both the success of contemporary dispersion-inclusive DFT methods for small noncovalent dimers, as well as unresolved discrepancies for larger complexes. For smaller systems, we show that the best DFT methods offer not only sub-kcal/mol accuracy but also reasonable consistency amongst themselves (Section 2), a conclusion that is echoed in other recent work *(144)*. Interpretative issues with DFT dispersion corrections are more subtle and are tackled in Section 3, where we address the extent to which a genuine dispersion energy can be extracted from a DFT calculation. Comparison to benchmark data for larger systems (Section 4) paints a rather different picture of DFT for vdW complexes, manifesting larger errors and clear differences between methods, albeit not necessarily systematic ones. We conclude with a look to the future in Section 5.

2. Present state-of-the-art in noncovalent DFT

In Section 2.1 we provide an overview of various strategies to augment DFT with dispersion interactions. We also describe the functionals that are used in the present chapter to provide a broad survey of the performance of contemporary DFT. The accuracy of these methods for small dimer benchmarks is reviewed in Section 2.2.

2.1 Strategies for dispersion interactions

2.1.1 Dispersion-inclusive XC functionals

Construction of dispersion-inclusive XC functionals has been reviewed elsewhere *(16,31,32,145)*. How this is accomplished will not be discussed in the present work, although we will make a few remarks about the functionals that are available.

When it comes to nonlocal electron correlation, as required by the physics of dispersion, there are only a few functionals to be found in the literature. The first among these was vdW-DF04 *(17)*, sometimes called vdW-DF1 *(32)*, which was later reformulated into an improved version known as vdW-DF2 *(19)*. It has since spawned other variants that use the same nonlocal correlation model *(20,146–152)*. That model employs a

numerically tabulated kernel, which delayed the self-consistent implementation of vdW-DF *(153–155)*. A simpler nonlocal correlation functional, with an analytic construction, was developed later by Vydrov and Van Voorhis and is known as VV10 *(23)*, superseding a predecessor called VV09 *(22)*, and with a revision called rVV10 that is better suited for plane-wave basis sets *(156)*. The analytic construction of VV10, combined with poor performance of vdW-DF04 when paired with hybrid XC functionals *(154)*, likely accounts for the more widespread adoption of VV10 in molecular applications, although rVV10 has been incorporated into functionals designed for the solid state *(157–160)*. For molecules, which are the focus of the present chapter, a notable use of VV10 is its incorporation into the highly successful B97-based *(161)* functionals developed over the past decade by Mardirossian and Head-Gordon *(25–29)*.

Some meta-GGA functionals that lack nonlocal correlation have also been advocated as DFT solutions for noncovalent problems, particularly those in the "Minnesota" class of meta-GGAs *(162–164)*, and especially M05-2X *(165)* and M06-2X *(75)*. As meta-GGAs, the Minnesota functionals include a dependence on both the density Laplacian and the kinetic energy density *(166)*, and as a result their (still local) kernels may extend farther from the nuclei as compared to functionals on lower rungs of Jacob's Ladder. The practical result is that semilocal meta-GGA XC effects are nonzero at vdW contact distances, therefore some attractive interactions are built into their parameterization, mimicking dispersion at typical vdW separations even if true long-range dispersion is missing *(86)*. This contrasts what is observed for PBE and B3LYP in Fig. 1, where interaction potentials for $(C_6H_6)_2$ and Kr_2 are strictly repulsive. Notably, the Minnesota functionals are highly parameterized even as compared to other empirical XC functionals *(30)*.

For the present overview, we selected a small set of XC functionals that perform especially well for noncovalent interaction energies according to a recent comprehensive review *(30)*. The best-performing functionals are mostly (though not exclusively) meta-GGAs. The smallest overall root-mean-square error (RMSE) for noncovalent interaction energies is 0.2 kcal/mol for the ωB97M-V functional *(26)*, but several other meta-GGAs also have RMSEs below 0.5 kcal/mol including ωB97X-V *(25)*, M06-2X *(75)*, TPSSh *(167)*, and B97M-rV *(28)*. These are functionals that are designed to capture dispersion from first principles, without the use of *ad hoc* corrections, although a variety of functionals that include such corrections have error statistics that are equally impressive *(30)*. Double-hybrid functionals *(168–171)*, which include

a fraction of the correlation energy from second-order Møller-Plesset (MP2) perturbation theory, will not be considered because they fundamentally alter the cost and thus the efficacy of DFT calculations. Moreover, finite-order MP*n* theory affords troubling divergences for nanoscale vdW complexes that may be inherited by double-hybrid functionals *(172)*. The performance of double-hybrids for noncovalent interactions is discussed elsewhere *(88,169,173–176)*.

It is important to note that meta-GGA functionals often exhibit more acute dependence on the numerical integration scheme as compared to functionals on lower rungs of Jacob's Ladder. Noncovalent interactions are especially sensitive in this regard because they depend on small oscillations in the tails of the electron density, characterized by large values of the reduced density gradient *(177–179)*,

$$s(\mathbf{r}) = \frac{\|\hat{\nabla}\rho(\mathbf{r})\|}{2(3\pi^2)^{1/3}\rho(\mathbf{r})^{4/3}}. \tag{1}$$

Minnesota meta-GGAs are especially problematic in terms of how results for noncovalent interactions depend on the quadrature grid *(180–184)* and sometimes behave erratically in the CBS limit *(185–187)*. We use the SG-3 quadrature grid for Minnesota functionals and the SG-2 grid for other meta-GGAs *(183)*. (Consistent with previous testing *(188)*, we find that the SG-2 grid is sufficient for the SCAN functional despite its well-documented grid sensitivity *(189)*).

We will also use the PBE, PBE0 *(190)*, B3LYP, and SCAN *(191)* functionals as starting points for adding dispersion corrections that are discussed in more detail in Section 2.1.2. With the exception of SCAN, these functionals perform quite poorly for noncovalent interactions, to the point of affording strictly repulsive potentials for systems where dispersion is qualitatively important (Fig. 1). However, they can still serve to set a baseline for the effectiveness of dispersion corrections. Many other functionals could be found whose errors for noncovalent data sets are much larger, but it is not our intention to provide a broad survey of poor choices.

2.1.2 Dispersion-corrected approaches

We next elaborate the various *ad hoc* dispersion corrections that have been developed to augment semilocal and hybrid DFT. Empirical dispersion corrections in DFT+D can be written in generic form as

$$E_{\mathrm{DFT+D(0)}} = E_{\mathrm{DFT}} \underbrace{-s_n \sum_{n=6,8,\ldots} \sum_{a}^{\text{atoms}} \sum_{b>a}^{\text{atoms}} f_n\left(R_{ab}\right) \frac{C_{n,ab}}{R_{ab}^{n}}}_{+\mathrm{D(0)}}, \tag{2}$$

where E_{DFT} represents the DFT energy and the rest is a dispersion correction. Only the C_6 and C_8 terms in Eq. (2) are included in Grimme's popular D3 and D4 models *(36,37)*, as higher-order terms are found to engender numerical problems while providing little improvement *(36)*. Parameters $s_n \leq 1$ are functional-specific and the damping functions f_n are chosen such that $f_n(R) \to 0$ faster than R^n, so that the correction is damped to zero as $R \to 0$. This has been called the "zero-damping" form of DFT+D *(192)*, and that is the meaning of the notation DFT+D(0) in Eq. (2). Various damping functions f_n have been considered *(125,192–194)*.

An alternative to D(0) damping is the "D(BJ)" correction scheme *(192)*, first introduced by Becke and Johnson (BJ) in the context of the XDM model *(45–47)*. In DFT+D(BJ), one corrects the DFT energy according to

$$E_{\mathrm{DFT+D(BJ)}} = E_{\mathrm{DFT}} \underbrace{-s_n \sum_{n=6,8,\ldots} \sum_{a}^{\text{atoms}} \sum_{b>a}^{\text{atoms}} \frac{C_{n,ab}}{R_{ab}^{n} + \left(R_{ab}^{\mathrm{vdW}}\right)^{n}}}_{+\mathrm{D(BJ)}}. \tag{3}$$

This is similar to Eq. (2) but uses pairwise vdW radii (R_{ab}^{vdW}) to prevent divergence as $R_{ab} \to 0$, in place of damping functions f_n. These radii are parameterized according to

$$R_{ab}^{\mathrm{vdW}} = a_1 R_{ab}^{0} + a_2 \tag{4}$$

where a_1 and a_2 are empirical parameters. In principle, R_{ab}^{0} might also be an empirical parameter, equal to the sum of vdW radii of atoms a and b. In practice, the choice works well *(192)*.

$$R_{ab}^{0} = \left(C_{8,ab} / C_{6,ab}\right)^{1/2} \tag{5}$$

Regardless of the particulars of the dispersion damping, at a fundamental level the atom–atom C_6 coefficients come from the Casimir-Polder relation *(31,195,196)*

$$C_{6,ab} = \frac{3\hbar}{\pi} \int_0^{\infty} \bar{\alpha}_a(\mathrm{i}\omega)\, \bar{\alpha}_b(\mathrm{i}\omega)\, d\omega. \tag{6}$$

Here, the isotropic polarizability $\bar{\alpha}_x$ for atom x is evaluated at imaginary frequency $\mathrm{i}\omega$. In the D3 model *(36)*, values for $C_{6,ab}$ that depend on

coordination numbers of atoms a and b are obtained by applying Eq. (6) to model compounds, with polarizabilities computed using time-dependent (TD-)DFT. In the D4 model *(37)*, these polarizabilities are further scaled based on Mulliken charges obtained from the SCF density, which provides additional dependence on the molecular environment. Higher-order C_n coefficients, representing higher-order multipolar contributions to dispersion, can be approximated in terms of C_6 coefficients *(36,48,197,198)*.

The DFT+D3 and DFT+D4 models both incorporate Dobson's type-A nonadditivity (meaning C_n coefficients that depend on the molecular environment) but neglect type-B nonadditivity (screening of the pairwise interactions by other polarizable centers) *(53)*. As a result, the pairwise-additive approximations in Eqs. (2) and (3) break down for larger molecules *(54–56,128)*. To correct for this, an ATM correction can be added, representing the leading-order contribution to three-body dispersion *(58,59)*. In the D3 model, for example, this correction takes the form *(36)*

$$E_{3B}^{ATM} = -\sum_{a}^{atoms}\sum_{b>a}^{atoms}\sum_{c>b}^{atoms}\frac{g_{abc}\,C_{9,abc}\,f_{3B}\,(\bar{R}_{abc})}{R_{ab}^3 R_{ac}^3 R_{bc}^3} \tag{7}$$

where g_{abc} is a geometric factor and $f_{3B}\,(\bar{R}_{abc})$ is a damping function that depends on the mutual three-body distance, $\bar{R}_{abc}$ *(56)*. The requisite C_9 coefficients can be estimated from the C_6 coefficients *(36)*,

$$C_{9,abc} = (C_{6,ab}\,C_{6,bc}\,C_{6,ac})^{1/2}. \tag{8}$$

Separate from Grimme's D3 and D4 corrections, other formulations of DFT+D aim to incorporate type-A nonadditivity using the full SCF density rather than the density for a model compound or density-derived point charges. These alternatives include the XDM *(46,48)*, MBD *(60,61)*, and vdW-TS *(51)* dispersion corrections, each of which computes *in situ* C_6 coefficients in similar ways that take advantage of the relationship between polarizability and volume *(199–201)*. Specifically, one may determine an effective atom-in-molecule polarizability for atom a ($\bar{\alpha}_a^{\text{eff}}$) by scaling the free-atom polarizability ($\bar{\alpha}_a^{\text{free}}$) by a ratio equal to how the volume of a is compressed in its molecular environment *(46)*:

$$\bar{\alpha}_a^{\text{eff}} = \left(\frac{\langle r^3\rangle_a}{\langle r^3\rangle_a^{\text{free}}}\right)\bar{\alpha}_a^{\text{free}}. \tag{9}$$

The quantity $\langle r^3\rangle_a$ may be interpreted as the volume occupied by atom a within the molecular environment, and it is computed via Hirshfeld

partition of the SCF density *(46,48,202–204)*. The Hirshfeld technique *(205)*, which is more often associated with atomic partial charges *(143,206–209)* integrates the molecular SCF density $\rho(\mathbf{r})$ using a weighting function $w_a(\mathbf{r})$ for atom a. This function is obtained by considering where (in space) atom a contributes to the superposition of free-atom densities, $\sum_b \rho_b^{\text{free}}(\mathbf{r})$, and is given by

$$w_a(\mathbf{r}) = \frac{\rho_a^{\text{free}}(\mathbf{r})}{\sum_b \rho_b^{\text{free}}(\mathbf{r})}. \tag{10}$$

The volume needed in Eq. (9) is computed according to *(46)*

$$\langle r^3 \rangle_a = \int r^3 w_a(\mathbf{r})\, \rho(\mathbf{r})\, d\mathbf{r}. \tag{11}$$

Using effective polarizabilities $\bar{\alpha}_a^{\text{eff}}$ obtained from Eq. (9), Becke and Johnson proposed a model for $C_{6,ab}$ that is expressed in terms of the dipole moment of the exchange hole, $\mathbf{d}_x(\mathbf{r})$. That quantity depends on position, because the hole is a function of the position of a reference electron, but the exchange-hole dipole moment enters the Becke-Johnson model as its spherically averaged second moment, $\langle d_x^2 \rangle$. The model for $C_{6,ab}$ is *(46,48)*.

$$C_{6,ab}^{\text{BJ}} = \frac{\bar{\alpha}_a^{\text{eff}}\, \bar{\alpha}_b^{\text{eff}}\, \langle d_x^2 \rangle_a \langle d_x^2 \rangle_b}{\bar{\alpha}_b^{\text{eff}} \langle d_x^2 \rangle_a + \bar{\alpha}_a^{\text{eff}} \langle d_x^2 \rangle_b}. \tag{12}$$

Additional theoretical and numerical support for this model were provided later *(204,210)*. With the help of recursion relations for the higher-order dispersion coefficients *(46,48)*, Eq. (12) forms the basis of a DFT+D model of the form in Eq. (3) and consisting of C_6, C_8, and C_{10} terms where each C_n coefficient reflects the molecular environment. This is the Becke-Johnson XDM approach. Parameters for R_{ab}^{vdW} in Eq. (4) have been determined for a variety of XC functionals *(211)*.

In the vdW-TS scheme *(51)*, a relationship analogous to Eq. (9) is assumed for the effective atomic C_6 coefficients,

$$C_{6,a}^{\text{eff}} = \left(\frac{\langle r^3 \rangle_a}{\langle r^3 \rangle_a^{\text{free}}} \right) C_{6,a}^{\text{free}}, \tag{13}$$

with free-atom coefficients $C_{6,a}^{\text{free}}$ taken from TDDFT calculations *(212)*. Pairwise C_6 coefficients are then obtained according to

$$C_{6,ab}^{\mathrm{TS}} = \frac{2\, C_{6,a}^{\mathrm{eff}}\, C_{6,b}^{\mathrm{eff}}}{(\bar{\alpha}_b^{\mathrm{free}}/\bar{\alpha}_a^{\mathrm{free}})\, C_{6,a}^{\mathrm{eff}} + (\bar{\alpha}_a^{\mathrm{free}}/\bar{\alpha}_b^{\mathrm{free}})\, C_{6,b}^{\mathrm{eff}}}. \tag{14}$$

This form for $C_{6,ab}$ can be derived from Eq. (6) based on a single-frequency model for the isotropic atomic polarizabilities *(51,213)*,

$$\bar{\alpha}_a^{\mathrm{TS}}(\mathrm{i}\omega) = \frac{\bar{\alpha}_a^{\mathrm{free}}}{1 + (\omega/\omega_a)^2}. \tag{15}$$

Here, ω_a is a characteristic excitation frequency whose value is set at

$$\omega_a = \frac{4C_{6,a}}{3\hbar(\bar{\alpha}_a^{\mathrm{free}})^2}. \tag{16}$$

This choice recovers London's formula *(213)*,

$$C_{6,ab} = \frac{3\omega_a\omega_b\bar{\alpha}_a\bar{\alpha}_b}{2(\omega_a + \omega_b)} \approx \frac{3I_aI_b\bar{\alpha}_a\bar{\alpha}_b}{2(I_a + I_b)} \tag{17}$$

starting from Eq. (6) *(51)*. For small molecules, the characteristic frequencies in Eq. (17) are typically further approximated by ionization energies (I_a and I_b), as indicated, which affords the textbook result *(145)*.

The single-frequency model in Eq. (15) is tantamount to the Unsöld approximation *(214–218)*, in which energy denominators are replaced by a single effective excitation energy so that a sum-over-states expression for the polarizability reduces to a single term *(218)*. This approximation enters London's second-order treatment of dispersion *(32)* and is found to work well *(217,218)*, hence there is a natural consistency to its use in the present context. It is worth noting that a single-frequency or "plasmon-pole" approximation for the inverse dielectric function is used to construct both the vdW-DF and VV10 nonlocal correlation functionals *(14,22,37)*.

The vdW-TS scheme uses $C_{6,ab}$ in Eq. (14) within the DFT+D(0) model of Eq. (2), although it has also been implemented as a self-consistent functional based on a $C_{6,ab}[\rho(\boldsymbol{r})]$ functional *(219)*. Like XDM, the vdW-TS approach affords pairwise C_6 coefficients that depend on the molecular environment, meaning that type-A nonadditivity is included in the model. We will not consider the vdW-TS scheme in the present work because it is largely superseded by the MBD model developed subsequently by Tkatchenko and co-workers *(60,61)*. Starting from the vdW-TS polarizability model in Eq. (15), the MBD approach further accounts for type-B nonadditivity based on self-consistent screening (SCS) of the atomic polarizabilities. These many-atom dispersion effects may be especially

important for large, conjugated molecules and in materials having numerous polarizable centers *(220–224)*. In nanoscale materials, many-body effects lead to deviations from R^{-6} behavior in the long-range interactions *(225–227)*.

Development of the MBD method starts from the atomic polarizability model in Eq. (15), arranged as a vector $\bar{\boldsymbol{\alpha}}^{\mathrm{TS}}$ of dimension N_{atoms}. (In polarizable force fields, even anisotropic molecular polarizabilities are found to be well described by *isotropic* atom-centered distributed polarizabilities *(228–231)*, as the short-range damping that is necessary to avoid divergence also has the effect of reducing the polarizability along the direction of covalent bonds *(232)*). Allowing for mutual dipole–dipole interactions between the atomic centers, which is consistent with a model that includes only dipole polarizabilities, leads to a self-consistent screening (SCS) *ansatz (61)*,

$$\bar{\boldsymbol{\alpha}}^{\mathrm{SCS}}(\mathrm{i}\omega) = \bar{\boldsymbol{\alpha}}^{\mathrm{TS}} - \bar{\boldsymbol{\alpha}}^{\mathrm{TS}}\mathbf{T}_{\mathrm{SR}}\bar{\boldsymbol{\alpha}}^{\mathrm{SCS}}(\mathrm{i}\omega). \tag{18}$$

Here, $\mathbf{T}_{\mathrm{SR}}$ is a short-range version of the dipole-interaction tensor *(61)*, consistent with the idea that short-range correlation will be captured by semilocal DFT leaving only the long-range component for the dispersion model. To that end, and noting that a single, isotropic quantum harmonic oscillator can capture C_6 *(32)*, the MBD model consists of a $3N_{\mathrm{atoms}}$-dimensional harmonic oscillator Hamiltonian, with a three-dimensional (but isotropic) oscillator on each atom. Polarizabilities are determined by self-consistent solution of Eq. (18) *(60)*. Unlike other dispersion-corrected DFT methods described in this section, MBD does not use either of the DFT+D formulas in Eqs. (2) and (3). Instead, the correction to conventional DFT emerges as the ground-state energy of the harmonic oscillator Hamiltonian, eigenmodes of which provide information about collective or many-body contributions to dispersion *(70,223)*.

2.2 Benchmarks for small noncovalent dimers

Many comprehensive assessments of modern DFT are available, based upon small noncovalent dimer data sets *(83–89)*. In Section 2.2.1, we briefly consider the performance of selected methods for the S66 set *(119)*, in order to establish that sub-kcal/mol accuracy is a reality in contemporary DFT for small vdW complexes. Section 2.2.2 considers the role of basis-set superposition error (BSSE).

Except in our discussion of BSSE, where some smaller basis sets are examined for demonstrative purposes, all of the DFT calculations reported

here are performed near the CBS limit, in order to ascertain the true performance of DFT for noncovalent interactions. Unless stated otherwise, all DFT calculations use the def2-QZVPD basis set *(233)*, except that DFT+XDM calculations use the aug-cc-pVTZ basis set *(234)*, following a literature recommendation *(235)*. All DFT interaction energies include Boys-Bernardi counterpoise (CP) correction *(88,236,237)* Benchmarks tests establish that quadruple-ζ basis sets are sufficient to obtain the DFT/CBS limit for noncovalent interactions *(88,185,238)*, except for a few especially problematic Minnesota functionals *(88,185)*. At the DFT/def2-QZVPD level, CP correction typically modifies E_{int} by $\sim$0.1 kcal/mol, which establishes that the DFT/CBS limit has been reached. The use of DFT/CBS interaction energies prevents basis-set artifacts from clouding the discussion.

XC functionals were introduced in Section 2.1. Following the recommendation of Grimme et al. *(192)*, all of the DFT+D methods in this work use the D(BJ) damping scheme of Eq. (3) except in the case of dispersion-corrected M06-2X. Per other recommendations *(30)*, we use M06-2X+D(0) in that case.

2.2.1 Error analysis for the S66 data set

The S66 dimers range in size from $(H_2O)_2$ up to pentane dimer and are divided into three subsets based on the ratio of the electrostatic energy (E_{elst}) to the dispersion energy (E_{disp}), as determined using symmetry-adapted perturbation theory (SAPT). Dimers where $|E_{\text{elst}}| \geq 2|E_{\text{disp}}|$ are classified as hydrogen-bonded, those where $|E_{\text{disp}}| \geq 2|E_{\text{elst}}|$ are categorized as dispersion-dominated, and if neither of these condition is met then the system is regarded as having mixed-influence interactions *(119)*. Although SAPT is used to classify the dimers, benchmark interaction energies have been determined at the CCSD(T)/CBS level *(119)*.

Figure shows the calculated S66 interaction energies for a wide variety of functionals, plotted alongside the reference values. These DFT results include "baseline" functionals that lack any dispersion correction and thus fail to bind most of the dispersion-dominated dimers. Even for the hydrogen-bonded subset of S66, however, these baseline functionals systematically underestimate the interaction energies, by $\gtrsim 1$ kcal/mol in many cases. (Errors are considerably larger for the other subsets of S66.) In contrast, results obtained using dispersion-inclusive functionals track the reference values exceedingly well, to the point that we have not attempted to break out the performance of individual functionals in Fig. 2.

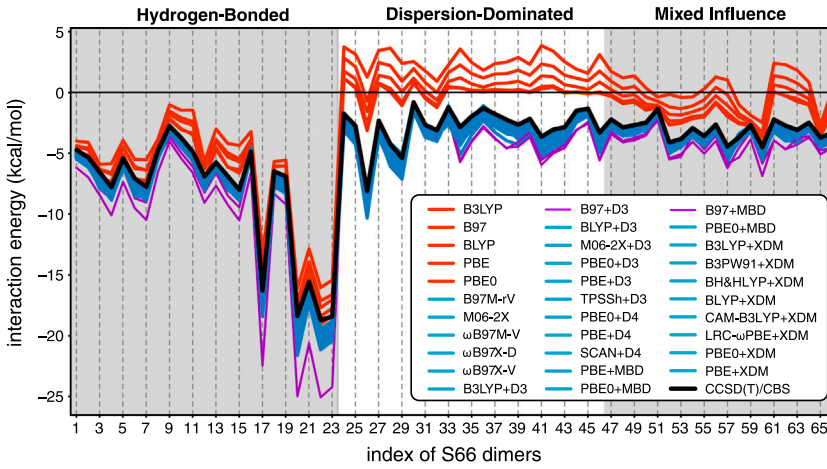

Fig. 2 Interaction energies for the S66 data set determined using DFT/def2-QZVPD calculations, except for DFT+XDM where the aug-cc-pVTZ basis set was used. CCSD(T)/CBS reference values are also shown *(119)*. Functionals without a dispersion correction are shown in orange and are typically unbound for the dispersion-dominated complexes. Dispersion-inclusive DFT methods are shown in blue and purple, with purple used for B97+D3 and B97+MBD where the mean absolute error exceeds 1 kcal/mol.

Error statistics for individual functionals appear in Fig. 3. Throughout this work, we define

$$\text{error} = E_{\text{DFT}} - E_{\text{benchmark}}, \tag{19}$$

which establishes our sign convention. Of all the functionals that we tested, only the ones lacking dispersion corrections afford mean absolute errors (MAEs) larger than 1 kcal/mol, with the exception of B97+D3 and B97+MBD. In the absence of any dispersion correction, average signed errors (Fig. 3B) range up to 3.5 kcal/mol (for BLYP), which is quite large considering that the average CCSD(T)/CBS interaction energy for the S66 complexes is only 4.8 kcal/mol.

It is interesting that all of the dispersion-inclusive approaches overestimate the interaction energies. Unlike the underbinding observed in the absence of dispersion corrections, which is entirely predictable, overbinding by dispersion-inclusive approaches would not seem to be built in by design but emerges nonetheless. The effect is rather small, however. Setting aside B97+D3 and B97+MBD, the differences in error statistics from one functional to the next are smaller than the statistical errors with respect to the reference values, and in that sense the accuracy of these

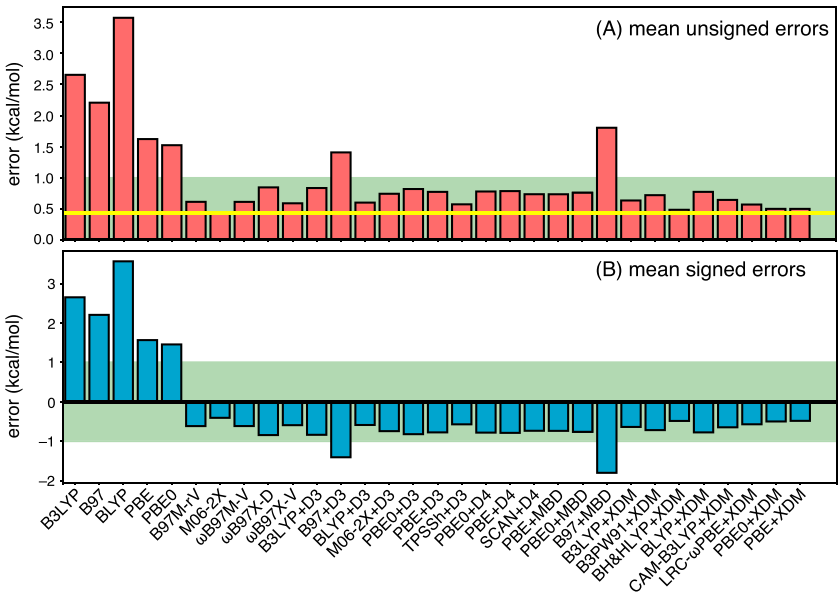

Fig. 3 (A) Mean absolute errors (MAEs) and (B) mean errors (signs included) for DFT-based interaction energies averaged over the S66 data set. These statistics correspond to the data plotted in Fig. 2. Error is measured relative to CCSD(T)/CBS reference values [Eq. (19)], with ± 1 kcal/mol indicated by the colored region. M06-2X exhibits the lowest MAE in this data set and that value is indicated by the horizontal line in (A).

dispersion-inclusive hybrid and meta-GGA functionals is statistically indistinguishable. Consistent with other statistical assessments *(83–89)* these results demonstrate unequivocally that DFT provides interaction energies of sub-kcal/mol accuracy for small vdW dimers.

2.2.2 BSSE and counterpoise correction

Results presented above were computed near the CBS limit but quadruple-ζ basis sets may not be feasible for nanoscale vdW complexes, not only for reasons of cost but also due to numerical linear dependencies that necessitate increasingly tight thresholds as molecular size increases, especially in the presence of diffuse basis functions *(239)*. Fortunately, CP correction can substantially mitigate the need for large basis sets, according to a comprehensive analysis of CP-corrected DFT calculations *(88)*, and CP-DFT/double-ζ interaction energies are found to be comparable to DFT/CBS values.

Convergence to the DFT/CBS limit is illustrated in Fig. 4 using the S66 data set. The CP-corrected and uncorrected interaction energies

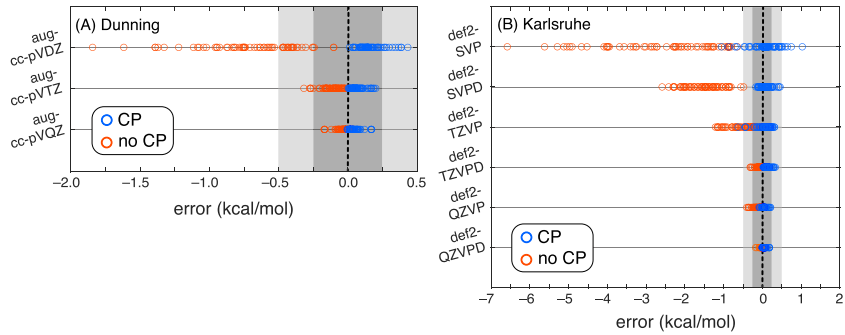

Fig. 4 Convergence errors (with respect to the DFT/CBS limit) for S66 interaction energies, using the B3LYP+D3(BJ) functional in (A) Dunning basis sets and (B) Karlsruhe basis sets. The gray rectangles delineate errors of ± 0.25 and ± 0.50 kcal/mol. *Reproduced with permission from Gray, M.; Bowling, P. E.; Herbert, J. M. Systematic Evaluation of Counterpoise Correction in Density Functional Theory. J. Chem. Theory Comput.* ***2022,*** *18, 6742–6756; copyright 2022 American Chemical Society.*

Table 1 BSSE in sizable vdW complexes, computed using ωB97M-V with various basis sets.[a]

Complex[b]	N_{atoms}	BSSE (kcal/mol)		
		def2-SVPD	def2-TZVPD	def2-QZVPD
$(C_{24}H_{12})_2$	72	11.5	0.8	0.3
$(pT)_5(C_{38}H_{22})(pT)_5$	134	36.0	2.7	—
$(pT)_5(C_{59}H_{20})(pT)_5$	153	43.4	3.2	—
$(pT)_7(C_{46}H_{26})(pT)_7$	174	47.3	3.3	—

[a]Data taken from Gray, M.; Bowling, P. E.; Herbert, J. M. Systematic Examination of Counterpoise Correction in Density Functional Theory. *J. Chem. Theory Comput.* **2022,** *18*, 6742–6756. [b]$(pT)_n$ is an n-unit polythiophene oligomer.

approach the CBS limit in opposite directions but CP-corrected results do so more quickly. With CP correction, an augmented double-ζ basis set is sufficient to get within 0.5 kcal/mol of the DFT/CBS limit, whereas in its absence an augmented triple-ζ basis set is needed to obtain a similar result.

BSSE is essentially a form of charge transfer between neighboring atoms, which grows with system size because so does the number of neighbors (meaning nearby pairs of atoms). This form of extensivity is illustrated in Table 1, which quantifies the BSSE for sizable vdW complexes in various basis sets. Here, BSSE is defined as

$$\mathrm{BSSE} = E_{\mathrm{CP-DFT}} - E_{\mathrm{DFT}}. \tag{20}$$

The complexes in Table 1 include the coronene dimer, $(C_{24}H_{12})_2$, and several trimers involving layered materials in which a graphene nanoribbon such as $C_{59}H_{20}$ is sandwiched between polythiophene oligomers, $(pT)_n$ *(240,241)*. Each of these layered composites exceeds 100 atoms and the BSSE computed at the ωB97M-V/def2-SVPD level exceeds 30 kcal/mol, approaching 50 kcal/mol for the largest example. This is 10–20× larger than the BSSE for any of the S66 complexes at the same level of theory *(88)*. For $(C_{24}H_{12})_2$, the BSSE is reduced below 1 kcal/mol when def2-TZVPD is used, but that is not true for the larger complexes considered in Table 1. In those cases, residual BSSE of about 3 kcal/mol persists in the def2-TZVPD basis set. For large vdW complexes, where basis sets beyond double-ζ quality may not be feasible, CP correction is thus critically important in order to obtain results that are even qualitatively reasonable. In addition, CP correction can partially mitigate the need for diffuse basis functions *(88)*.

3. Understanding dispersion in DFT calculations

Having established the accuracy of dispersion-inclusive DFT for noncovalent interactions, at least in small systems, we next use small-dimer data sets to examine the nature of the dispersion corrections themselves. A question arises as to what should constitute a benchmark dispersion energy, since DFT add-ons such as D3, D4, XDM, and MBD are defined as asymptotic corrections for long-range correlation, whereas middle-range correlation effects are contained within the XC functional. We will use the SAPT formalism to provide dispersion benchmarks, as described in Section 3.1, to which we compare the aforementioned *ad hoc* corrections in Section 3.2. Finally, in Section 3.3, we document the remarkable consistency of these *ad hoc* corrections for small dimers *(144)*.

All calculations in the present work are confined to the ground state. Recent benchmarks on noncovalent excimers *(242)*, considering relatively small systems ranging from benzene dimer to naphthalene and pyrene dimers, suggest that the *ad hoc* D3 and D4 dispersion corrections are less consistent for excited-state calculations using TDDFT. For excited states, specialized dispersion models may be required *(243)*, and this represents an avenue for future development. Excited-state SAPT methods, which might provide benchmark data, are only beginning to be developed *(244,245)*.

3.1 Dispersion benchmarks

The SAPT formalism has been reviewed elsewhere *(246–250)*. It provides a means to compute BSSE-free interaction energies (E_{int}) and to separate those quantities into physically meaningful components,

$$E_{\text{int}} = E_{\text{elst}} + E_{\text{exch}} + E_{\text{disp}} + E_{\text{ind}} \,, \tag{21}$$

providing a form of energy decomposition analysis (EDA). The components in Eq. (21) include electrostatics (E_{elst}), exchange or Pauli repulsion (E_{exch}), dispersion (E_{disp}), and induction (E_{ind}), the latter of which contains both polarization and charge transfer *(251)*. The elementary physics of these components is described elsewhere *(252–254)*. For the present discussion, it suffices to note that E_{disp} is cleanly separable from the remaining components, identifiable as a subset of the excitations in the perturbation series. This is different from the situation in methods such as DFT+D or DFT+MBD, where long-range dispersion is shouldered by the *ad hoc* correction but middle-range dispersion arises from the XC functional. The details of that separation depend sensitively on the length scale of the semilocal functional, which is difficult to assess *a priori (65)*.

In traditional SAPT, dispersion is defined in terms of simultaneous excitations on two individual monomers that create fluctuations in the charge density, leading to long-range multipolar interactions beyond those associated with any permanent multipole moments *(254)*. Equivalently, these fluctuations engender transient changes in the frequency-dependent polarizability *(252)*, and in either conceptual picture the dispersion interaction arises strictly from electron correlation *(254)*. At second order in intermolecular perturbation theory, which defines a variant known as "SAPT0" *(246,249)*, the total dispersion energy is a sum of second-order dispersion and exchange-dispersion terms *(249)*:

$$E_{\text{disp}}^{\text{SAPT0}} = E_{\text{disp}}^{(20)} + E_{\text{exch-disp}}^{(20)}. \tag{22}$$

Superscripts (*mn*) indicate *m*th-order perturbation theory with respect to the intermolecular Coulomb operator and *n*th-order in the Møller-Plesset fluctuation potentials for the monomers. The fact that $n = 0$ in Eq. (22) means that this approach is based on uncorrelated (Hartree-Fock) wave functions for the monomers. The exchange-dispersion term $E_{\text{exch-disp}}^{(20)}$ in Eq. (22) arises from the operator that enforces permutational antisymmetry between the monomer wave functions *(248,249)*.

The SAPT0 method affords a $-C_6/R^6$ dispersion effect, albeit not a quantitative one *(246,255–258)*, as it is generally too attractive *(68,255)*.

An improved approach that includes monomer electron correlation is SAPT2+ *(246,249)*, for which the dispersion energy is

$$E_{\text{disp}}^{\text{SAPT2+}} = E_{\text{disp}}^{\text{SAPT0}} + E_{\text{disp}}^{(21)} + E_{\text{disp}}^{(22)}. \tag{23}$$

Partial third-order calculations ($m = 3$) can provide CCSD(T)-quality interaction energies, via methods known as SAPT2+(3) and SAPT2+3 *(246,249)*. The corresponding dispersion energies are

$$E_{\text{disp}}^{\text{SAPT2+(3)}} = E_{\text{disp}}^{\text{SAPT2+}} + E_{\text{disp}}^{(30)} \tag{24}$$

and

$$E_{\text{disp}}^{\text{SAPT2+3}} = E_{\text{disp}}^{\text{SAPT2+(3)}} + E_{\text{exch-disp}}^{(30)}. \tag{25}$$

The third-order exchange-dispersion term in Eq. (25) is typically negligible unless the monomer separation is smaller than the vdW contact distance, or where ions are involved *(123)*; in other cases, SAPT2+(3) exhibits accuracy on par with CCSD(T) *(256,259)*. As such, $E_{\text{exch-disp}}^{(30)}$ is sometimes omitted from benchmark dispersion energies *(255)*. Note that SAPT2+ and SAPT2+(3) both exhibit $\mathcal{O}(N^7)$ complexity *(249,256)*, just like CCSD(T), which limits these methods to small systems.

An alternative approach is SAPT(DFT), which uses coupled Kohn-Sham response theory to obtain E_{disp} and is also found to agree well with the best wave function benchmarks *(247–249)*. By exploiting density fitting, the computational scaling of SAPT(DFT) calculations with hybrid XC functionals can be reduced to $\mathcal{O}(N^5)$ *(260)*, albeit with a much larger prefactor as compared to fifth-order methods such as MP2. SAPT(DFT) calculations on systems with 200 atoms have been demonstrated *(261)*, but few systematic benchmarks are available.

As a low-cost alternative that can yet provide well-defined dispersion energies, our group has developed a specialized form of the MBD Hamiltonian that is suitable for use with SAPT *(142,143,250)*. Because SAPT dispersion is defined at all length scales, this entails modifications to extend MBD to shorter length scales where the conventional MBD energy would be damped away; this is accomplished by incorporating dipole–quadrupole dispersion via screened C_8 coefficients *(142)*. The dispersion is still damped as $R \to 0$ but on a much shorter length scale as compared to the conventional version of MBD that is designed for use with DFT. The resulting SAPT+MBD approach affords excellent agreement with dispersion energies obtained from SAPT2+(3) *(262)*, despite a completely

different formalism, thus we deem it appropriate to use this version of MBD to provide dispersion benchmarks. These are easily obtainable for large systems as all that is required is diagonalization of a $(3N_{\text{atoms}}) \times (3N_{\text{atoms}})$ harmonic oscillator Hamiltonian matrix, as described in Section 2.1.2.

3.2 Interpretative issues in dispersion-corrected DFT

3.2.1 Does the +D correction have physical meaning?

To demonstrate that the numerical value of corrections such as D3 cannot be equated with genuine dispersion energies, Shahbaz and Szalewicz examined this corrections in comparison to a variety of SAPT benchmarks *(263,264)* (Fig. 5) plots several D3(BJ) corrections for Ar_2, as parameterized for several different XC functionals, alongside SAPT2+ dispersion energies. The D3(BJ) potential curves exhibit significantly shifted minima relative to $E_{\text{disp}}^{\text{SAPT2+}}(R)$. The former behave better asymptotically, because they are based on isolated-atom polarizabilities and should recover long-range dispersion, up to any intrinsic error associated with polarizabilities obtained from TDDFT. For a fixed value of R (say, the equilibrium separation

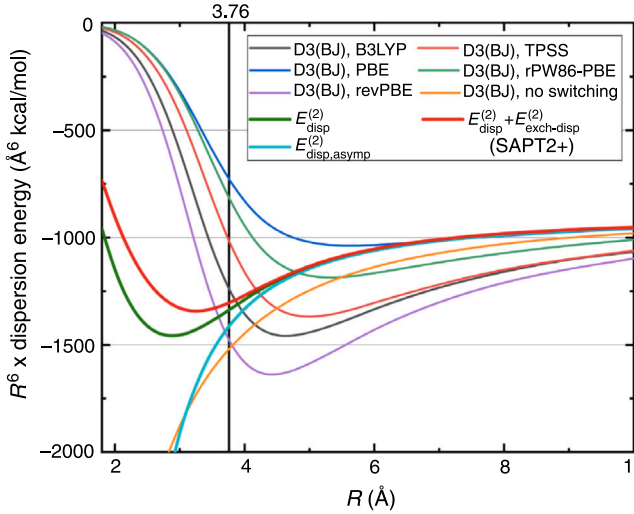

Fig. 5 D3(BJ) dispersion corrections and SAPT2+ dispersion energies for Ar_2, multiplied by R^6. The vertical line indicates the equilibrium separation when all of the energy components are considered. *Adapted with permission from Shahbaz, M.; Szalewicz, K. Do Semilocal Density-Functional Approximations Recover Dispersion Energies at Small Intermonomer Separations? Phys. Rev. Lett.* ***2018,*** *121, 113402; copyright 2018 American Physical Society.*

R = 3.76 Å that is indicated in Fig. 5), the D3(BJ) corrections exhibit a wide range of numerical values that may be larger or smaller than the SAPT2+ dispersion energy. Clearly, the numerical value of the D3(BJ) correction cannot be equated with dispersion and may not have physical meaning *(35)*. Others have reached the same conclusion in more systematic comparisons of D3(BJ) to SAPT *(265)*.

To avoid the inevitable intermingling of semilocal correlation and long-range empirical dispersion in the "middle-range" region (which is the length scale of typical vdW contact distances) *(34)*, Pernal et al. *(266)* developed a "dispersionless" density functional (dlDF) by reparameterizing M05-2X using a data set from which benchmark-quality SAPT dispersion energies had been subtracted from the data. Empirical corrections can be added to that functional (dlDF+D, using Grimme's D2 form) *(35)*, without concern about double-counting correlation. Fig. 6A demonstrates that this approach provides an accurate potential energy curve for Ar ⋯ Ne, much more so than the original M05-2X functional or the M06-2X functional, and also more accurate than B97+D *(266)*.

A similar approach has been used to develop empirical dispersion potentials to replace second-order dispersion in SAPT0. If a dispersion

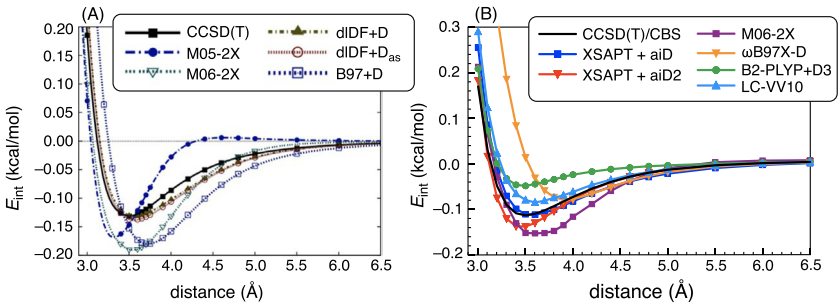

Fig. 6 Potential energy curves for Ar ⋯ Ne computed with various methods. (A) Comparison of dlDF+D with other dispersion-inclusive DFT methods, along with a CCSD(T) benchmark. The dlDF+D_{as} method includes additional SAPT dispersion data but is barely distinguishable from dlDF+D. (B) Comparison of XSAPT+aiD2 with DFT and CCSD(T). *(A) Adapted with permission from Pernal, K.; Podeszwa, R.; Patkowski, K.; Szalewicz, K. Dispersionless Density Functional Theory. Phys. Rev. Lett.* ***2009,*** *103, 263201; copyright 2009 American Physical Society. (B) Adapted with permission from Lao, K. L.; Herbert, J. M. An Improved Treatment of Empirical Dispersion and a Many-Body Energy Decomposition Scheme for the Explicit Polarization Plus Symmetry-Adapted Perturbation Theory (XSAPT) Method. J. Chem. Phys.* ***2013,*** *139, 034107; copyright 2013 American Institute of Physics.*

correction developed for DFT is used for this purpose, then its damping function must be adjusted in order to extend the range of the correction to shorter distances *(267,268)*, since there is no middle-range compensation from any XC functional. Alternatively, an empirical dispersion correction can be parameterized wholly from benchmark SAPT2+(3) or SAPT2+3 dispersion energies, to obtain an *ab initio* dispersion correction *(269–273)*. A method developed along these lines is SAPT+*ai*D *(56,250)*, where the nomenclature emphasizes that the dispersion correction is faithful to *ab initio* dispersion energies. SAPT+*ai*D is a cubic-scaling method with much better accuracy as compared to conventional SAPT0 *(258,272,273)*, which is a $\mathcal{O}(N^5)$ method, and it is demonstrated in Fig. 6B for the Ar ⋯ Ne system.

3.2.2 Energy decomposition analysis

We introduced the SAPT version of EDA in Section 3.1 as a means to obtain well-defined dispersion energies that are consistent with total interaction energies of CCSD(T) quality. There are numerous other EDA schemes within the quantum chemistry universe *(274–278)* however, and it is illuminating to ask whether any of them might clarify the physical nature of empirical dispersion corrections to DFT. That said, the inherent non-uniqueness of EDA models has led to controversy *(251,279–287)*, which is perhaps inevitable given that these models go beyond prediction of physical observables. To some extent, every EDA is a model that engages the question: "how many kJ/mol can dance on the head of a pin?". In what follows, we examine results using two common EDAs that are popular for DFT calculations: the second-generation EDA based on absolutely localized molecular orbitals (ALMO-EDA2) *(288–290)*, and the Ziegler-Rauk EDA *(291)* popularized by Bickelhaupt and Baerends *(292)*.

SAPT2+(3) dispersion benchmarks *(255,256)* are presented in Fig. 7A for the S22 data set *(117)*, plotted alongside ALMO-EDA2 and SAPT+MBD dispersion energies. The latter agree very well with the benchmarks, with a maximum difference of 0.9 kcal/mol and a MAE of 0.35 kcal/mol or 5%. As such, we will take the SAPT+MBD value of E_{disp} as a surrogate benchmark for the dispersion energy in large systems.

ALMO-EDA2 dispersion energies are quite different from benchmark values and typically much more attractive, so it is worth considering how these are computed. The original ALMO-EDA separates polarization in a well-defined way, leaving a "frozen" contribution to E_{int} that is comprised of the remaining energy components,

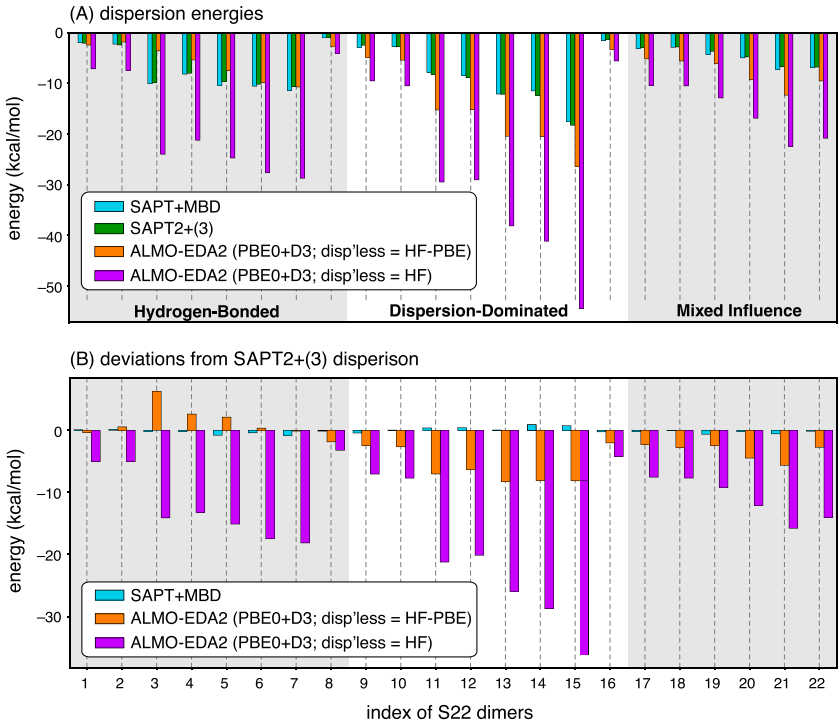

Fig. 7 (A) Dispersion energies for the S22 data set computed using various methods. (B) Difference between the SAPT+MBD *(262)* or ALMO-EDA2 dispersion energy and the SAPT2+(3)/aug-cc-pVTZ benchmark *(256)*. ALMO-EDA2 dispersion energies are computed using Eq. (27), with PBE0+D3 as the target functional and either HF or HF-PBE as the dispersionless functional, as indicated.

$$\Delta E_{\mathrm{FRZ}} = E_{\mathrm{elst}} + E_{\mathrm{exch}} + E_{\mathrm{disp}}. \tag{26}$$

To extract E_{disp} from ΔE_{FRZ}, it is suggested to use a functional that is (approximately) "dispersionless" *(289,290)*. Then, the dispersion energy for the target functional is estimated as the difference in ΔE_{FRZ} from two different calculations, one with the target (dispersion-inclusive) functional and one with the dispersionless functional:

$$E_{\mathrm{disp}}^{\mathrm{ALMO-EDA2}} = \Delta E_{\mathrm{FRZ}}^{\mathrm{target}} - \Delta E_{\mathrm{FRZ}}^{\mathrm{disp'less}}. \tag{27}$$

There could be various choices for the dispersionless functional, which creates some ambiguity. One might use the dlDF functional that was described in Section 3.2.1, although that seems not to have been tested. Instead, we follow literature recommendations *(289,290)*, which suggest

using Hartree-Fock (HF) exchange (without correlation) to compute the dispersionless value of ΔE_{FRZ} when a hybrid functional is the target, as for PBE0+D3 in Fig. 7. The dispersion energy estimated using Eq. (27) also contains any differences in how electrostatics and Pauli repulsion are described at these two levels of theory (PBE0+D3 versus HF), including any correlation effects in E_{elst} and E_{exch}. Other comparisons between SAPT and DFT-based EDA schemes suggest that correlation reduces E_{exch}, an effect that may mimic dispersion *(293)*. Whatever the reason, the aforementioned ALMO-EDA2 prescription for E_{disp} overshoots the SAPT2+(3) benchmark for every single S22 dimer (Fig. 7B), with a MAE of 14.0 kcal/mol or 209%.

The extent of this overestimation gives pause, and causes us to reconsider the choice of dispersionless functional. To prevent correlation effects in $E_{\mathrm{elst}} + E_{\mathrm{exch}}$ from contributing to E_{disp}, we consider using the HF-PBE functional,

$$E_{\mathrm{xc}}^{\mathrm{HF-PBE}} = E_{\mathrm{x}}^{\mathrm{HF}} + E_{\mathrm{c}}^{\mathrm{PBE}}, \tag{28}$$

to compute $\Delta E_{\mathrm{FRZ}}^{\mathrm{disp'less}}$. In conjunction with the same target functional (PBE0+D3), this choice significantly reduces the ALMO-EDA2 dispersion energies for the S22 dimers, bringing them closer to SAPT2+(3) benchmarks as shown in Fig. 7.

Linear regressions Fig. 8 demonstrate good correlation between SAPT+MBD dispersion energies and benchmark SAPT2+(3) values, with $R^2 = 0.99$ and a slope of 0.97. The ALMO-EDA2 dispersion energies also correlate with SAPT2+(3) values, using either HF or HF-PBE as the dispersionless functional, although they are systematically more attractive. Overall, HF-PBE works much better as the dispersionless functional as compared to the recommended choice of HF only. Using HF-PBE to define $E_{\mathrm{disp}}^{\mathrm{ALMO-EDA2}}$, the dispersion energies extracted from PBE0+D3 exhibit a MAE of 3.6 kcal/mol (54%) as compared to SAPT2+(3) reference values, albeit with significantly more scatter ($R^2 = 0.70$) as compared to SAPT+MBD dispersion energies. The primary difference between using HF or HF-PBE to compute $\Delta E_{\mathrm{FRZ}}^{\mathrm{disp'less}}$ lies in whether semilocal correlation effects are included in the dispersion energy (when HF is used), or whether they are removed (via HF-PBE). That the latter approach affords better agreement with benchmark dispersion energies suggests that semilocal correlation plays more of a role in electrostatics and Pauli repulsion than it plays in dispersion.

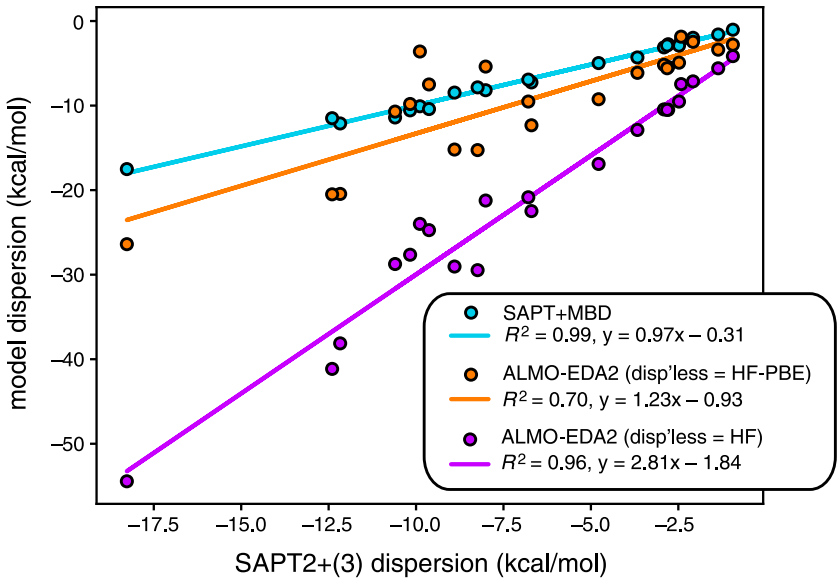

Fig. 8 Correlation between dispersion energies computed using either SAPT+MBD or ALMO-EDA2 and benchmarks computed at the SAPT2+(3)/aug-cc-pVTZ level. For ALMO-EDA2, two different "dispersionless" XC functionals are used to separate E_{disp} from ΔE_{FRZ} via Eq. (27). These are the same data as in Fig. 7A.

Energy components obtained from the Ziegler-Rauk EDA *(291,292)*, applied to DFT+D calculations, also correlate well with energy components from SAPT(DFT) *(265)*. These correlations are illustrated in Fig. 9 for the S66 dimers and they are quite remarkable in most cases, with the only exceptions being dispersion energies for hydrogen-bonded complexes ($R^2 = 0.706$) and induction energies for dispersion-dominated complexes ($R^2 = 0.565$). In those two cases, however, the energy component in question is quite small, and correlations improve significantly if E_{disp} and E_{ind} are summed, as suggested elsewhere *(294)*. Most importantly in the present context, the correlation between the D3(BJ) correction and the SAPT(DFT) dispersion energy is very strong for both the dispersion-dominated and mixed-influence subsets of S66, with $R^2 > 0.9$ in both cases, while the same is true for total interaction energies across all three subsets of S66 *(265)*. In these DFT+D calculations, which were performed using BLYP+D3(BJ), the authors simply equate E_{disp} with the numerical value of the D3(BJ) correction, which is compared in Fig. 9 to a scaled SAPT(DFT) dispersion energy computed in a double-ζ basis set. (The scaling is a correction for basis-set incompleteness *(295)*).

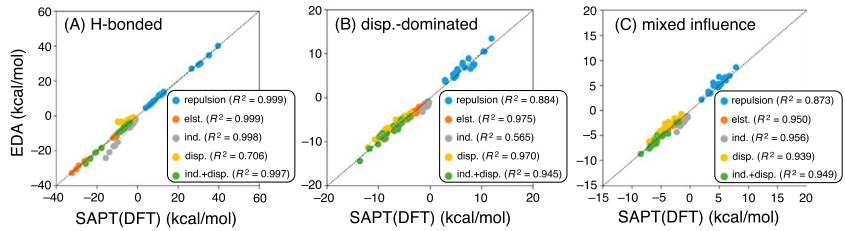

Fig. 9 Correlations between SAPT(DFT) energy components and those obtained from the Ziegler-Rauk EDA applied to BLYP+D3(BJ), for subsets of S66 including (A) hydrogen-bonded dimers, (B) dispersion-dominated complexes, and (C) mixed-influence dimers. The D3(BJ) correction is taken to represent E_{disp} in the DFT+D calculations. *Adapted with permission from Stasyuk, O. A.; Sedlak, R.; Guerra, C. F.; Hobza, P. Comparison of the DFT-SAPT and Canonical EDA Schemes for the Energy Decomposition of Various Types of Noncovalent Interactions. J. Chem. Theory Comput.* ***2018****, 14, 3440–3450; copyright 2018 American Chemical Society.*

The remarkable correlation between D3(BJ) and a genuine dispersion energy is reminiscent of ALMO-EDA2 when the HF-PBE functional is used to extract E_{disp} from a PBE0+D3(BJ) calculation. Together, these data suggest that not much of PBE or BLYP correlation actually accounts for dispersion, which is consistent with the purely repulsive potential energy profiles that these functionals often afford for dispersion-bound complexes (Fig. 1). Weaker interrelation between SAPT(DFT) dispersion and the D3(BJ) correction for hydrogen-bonded complexes reflects the fact that hydrogen bonds are associated with reduced intermolecular separation as compared to dispersion-dominated complexes (at equilibrium geometries), thus D3(BJ) is more strongly damped in hydrogen-bonded geometries and the XC functional must account for dispersion to a more significant extent than is required at the larger intermolecular separations representative of purely dispersion-bound complexes. At large separation, D3(BJ) does resemble genuine dispersion.

3.3 Consistency across different strategies

In view of the undeniable relationships between empirical dispersion corrections and genuine dispersion energies, as documented in Section 3.2.2, we embarked upon a more thorough comparison. Figure 10 examines SAPT+MBD dispersion energies for the S66 data set in comparison to D3, D4, XDM, and MBD corrections. Mirroring what was observed for the S22 data set, each of these corrections is systematically smaller (less attractive) as compared to SAPT+MBD dispersion. However, the corrections are rather

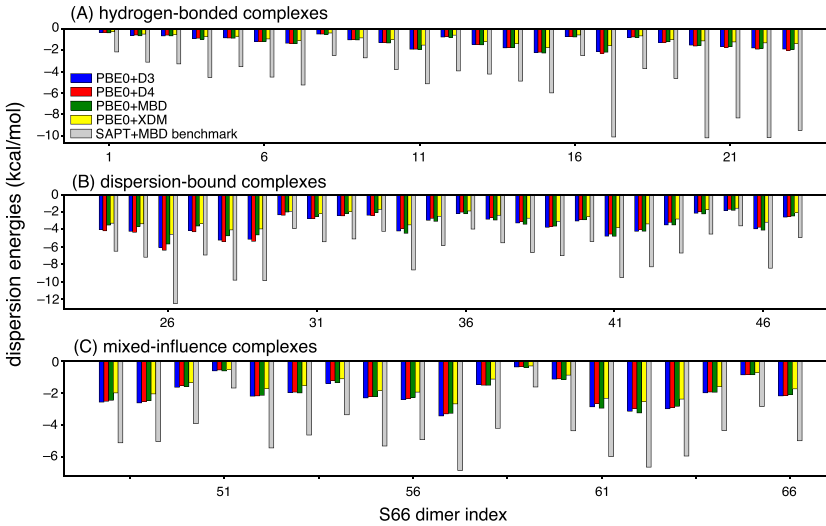

Fig. 10 Dispersion corrections (D3, D4, MBD, and XDM) for the PBE0 functional, evaluated for the S66 data set. Reference dispersion energies from SAPT+MBD are also shown. The S66 data set is separated into the usual subsets: (A) hydrogen-bonded complexes, (B) dispersion-dominated systems, and (C) dimers with mixed-influence interactions, and the same legend applies to all three panels.

consistent with one another, even if XDM is slightly less attractive than D3, D4, or MBD. The dispersion corrections are smaller for the hydrogen-bonded systems (defined by the condition $|E_{\text{elst}}| > 2|E_{\text{disp}}|$) as compared to the dispersion-dominated systems (where $|E_{\text{disp}}| > 2|E_{\text{elst}}|$), suggesting less long-range dispersion in the former.

The dispersion corrections do not afford (nor did we expect) quantitative agreement with genuine dispersion energies, represented here by SAPT+MBD, but qualitative correspondences are clear as demonstrated in Fig. 11. Very similar correlations are obtained using parameters appropriate for either PBE or PBE0, although the correlations are only qualitative ($R^2 \sim 0.6$) and there are several significant outliers. Linear regression affords slopes ranging from 0.33–0.45, consistent with the much smaller values of the long-range dispersion correction as compared to a genuine dispersion energy, underscoring the conclusion that the numerical value of a +D or +MBD dispersion correction should not be equated with E_{disp}. These are simply corrections to the DFT energy that improve the quality of potential energy surfaces for nonbonded systems, and are no less important simply because their numerical values do not have a direct physical interpretation at typical vdW contact distances.

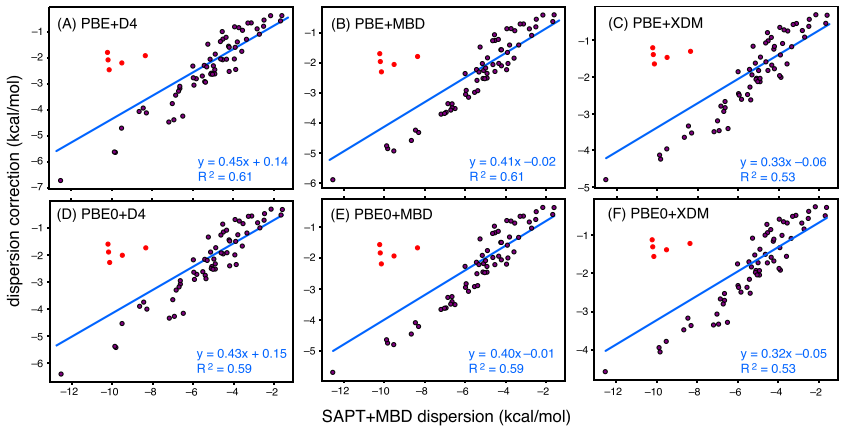

Fig. 11 Correlations between SAPT+MBD dispersion energies and DFT dispersion corrections (D3, D4, XDM, or MBD). The corrections are evaluated using PBE parameters in (A–C) and PBE0 parameters in (D–F). Blue lines are linear regressions and best-fit equations are indicated. These fits include the five outliers shown in red, each of which corresponds to a system containing two hydrogen bonds and a short intermolecular distance: $(\text{acetic acid})_2$, $(\text{acetamide})_2$, $(\text{uracil})_2$ in its base-pair geometry, (uracil) ⋯ (acetic acid), and (uracil) ⋯ (acetamide).

Johnson and co-workers recently published a comprehensive comparison of dispersion-corrected DFT methods (D3, D4, XDM, and MBD) *(144)*, using a database of 15,000 CCSD(T)/CBS noncovalent interaction energies, which is itself a subset of a larger database *(124)*. Both neutral and ionic complexes were considered and results are presented in (Fig. 12) in the form of histograms of errors in total interaction energies. The key take-home message is that a variety of correction schemes (as applied to the PBE0 functional in this case) afford very consistent results.

Examining the data for neutral systems first, MAEs are very consistent (at 0.49–0.50 kcal/mol) for all of the methods except vdW-TS, but even in that case the MAE is only 0.61 kcal/mol. RMSEs range from 0.8–0.9 kcal/mol for each method. Errors are larger for the ionic species but still quite consistent amongst methods, with MAEs ranging from 1.3–1.5 kcal/mol and RMSEs ranging from 1.75 kcal/mol (vdW-TS) to 2.09 kcal/mol (MBD). Maximum errors range from 7.85 kcal/mol (XDM) to 17.20 kcal/mol (MBD). Larger errors for ions are not surprising *(123)*, and the fact that the total spread of the RMSEs amongst these methods is only 0.3 kcal/mol is a remarkable measure of consistency, even if the maximum errors do span a range of about 9 kcal/mol. The mean variations between functionals are well within the intrinsic accuracy of any of them.

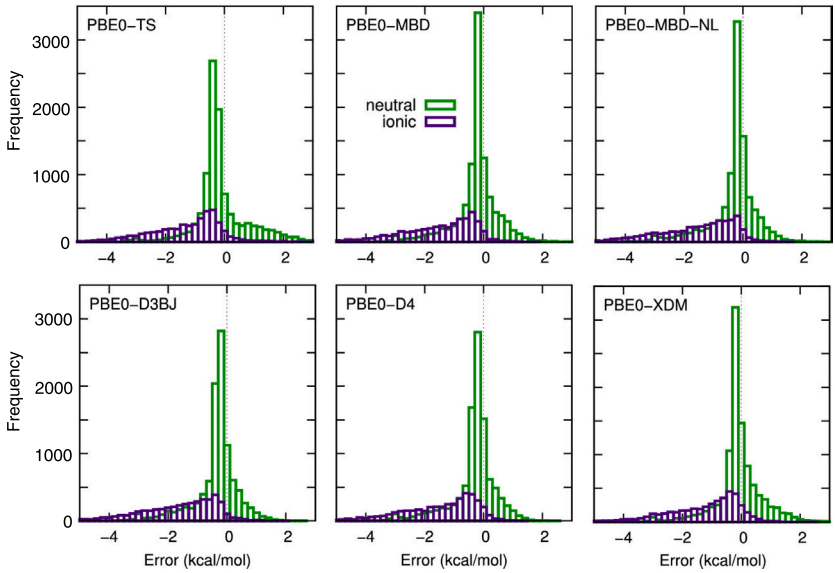

Fig. 12 Histograms of errors in dispersion-corrected DFT interaction energies as compared to CCSD(T)/CBS benchmarks, for the DES15K data set consisting of 15,000 noncovalent interaction energies *(124)*. Negative errors represent overbinding with respect to the benchmark. *Adapted with permission from Nickerson, C. J.; Bryenton, K. R.; Price, A. J. A.; Johnson, E. R. Comparison of Density-Functional Theory Dispersion Corrections for the DES15K Database. J. Phys. Chem. A2023, 127, 8712–8722; copyright 2023 American Chemical Society.*

Returning to the S66 data set, examination of the DFT dispersion corrections for individual systems illuminates an additional layer of consistency that cannot be gleaned from mere histograms of errors; see Fig. 13A. Comparing D3, D4, XDM, and MBD, as parameterized for the PBE functional in each case, we find that all four methods afford very similar corrections on a system-by-system basis. The largest differences are observed for the dispersion-dominated systems, whereas for the hydrogen-bonded dimers the variations are $\lesssim 0.5$ kcal/mol; see Fig. 13B. The XDM approach affords dispersion corrections at most variance to the other corrections but even so, these differences are no larger than 1.4 kcal/mol for any of the S66 dimers. The MAE between XDM and D3 is 0.4 kcal/mol, in systems where the magnitude of the total correction ranges up to 7 kcal/mol. This level of consistency is reassuring although perhaps not surprising, as the description of these models in Section 2.1.2 emphasized similarities in the construction of each. In the next section, however, we will find that this consistency does not extend to larger vdW complexes.

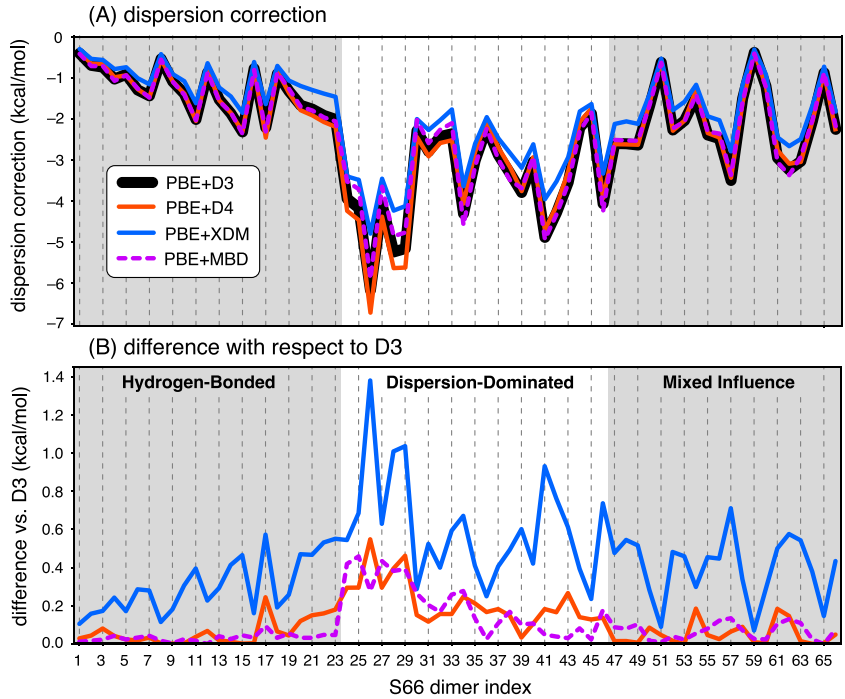

Fig. 13 (A) Dispersion corrections (parameterized for PBE) evaluated for the S66 data set. (B) Absolute difference between the D3 correction and the other dispersion corrections, for the same data set. The legend applies to both panels.

4. Results for large systems

Despite DFT's somewhat poor reputation for noncovalent interactions, the present work showcases that dispersion-inclusive and dispersion-corrected functionals achieve MAEs $\lesssim 0.5$ kcal/mol as compared to CCSD(T)/CBS benchmarks, for total interaction energies in small noncovalent dimers. Errors are larger, yet equally consistent, when those dimers are ionic. Dispersion corrections are not genuine dispersion energies in themselves yet they correlate quite well with benchmark dispersion energies from SAPT calculations.

These results prove to be a best-case scenario for DFT. We next examine larger systems, ranging up to nanoscale vdW complexes (Section 4.1), comparing DFT to what benchmarks are available. As for the smaller systems, we use CP-corrected DFT/def2-QZVPD interaction energies where feasible, in order to reveal the inherent performance of each functional. For the very

largest complexes, we will use CP-corrected DFT/def2-TZVPD calculations, which should still lie close to the DFT/CBS limit *(88)*. Following this comparison of DFT interaction energies to reference values, we will examine the magnitude of the dispersion corrections for these systems (Section 4.2) and the size of the CP corrections (Section 4.3). This discussion will paint a rather different picture as compared to what we have seen in small dimers.

4.1 Comparison to benchmarks

Within quantum chemistry, detailed investigation of noncovalent interactions in larger systems began about a decade ago with the introduction of the L7 *(127)* and S12L *(55,94)* test sets. The L7 complexes are depicted in (Fig. 14), to which we have added a 132-atom buckyball-in-a-ring system (C_{60}@[6]CPPA). The latter was taken from a recent study *(131)*, in which several of the complexes in (Fig. 14) are found to be problematic for methods well beyond DFT, affording disagreements amongst the best *ab initio* benchmarks. For C_{60}@[6]CPPA, guanine–cytosine on circumcoronene (C3GC), and the parallel-displaced coronene dimer (C2C2PD), benchmark interaction energies obtained from fixed-node diffusion Monte Carlo (FN-DMC) calculations disagree with CCSD(T)/CBS results *(131)*. The CCSD(T) calculations were performed using a local-orbital approximation, in this case localized natural orbital (LNO-)CCSD(T) *(296–299)*, and such approximations are not without sources of error *(299–304)*. Those errors can be estimated, however, and the discrepancies with respect to FN-DMC interaction energies lie outside of the combined error bars of

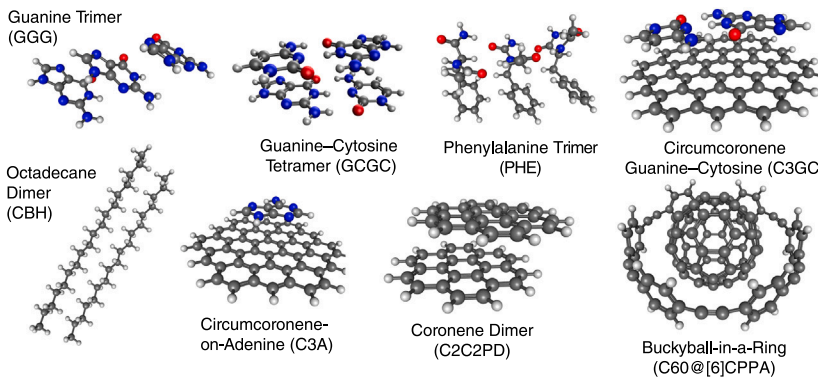

Fig. 14 Larger vdW complexes considered herein. The first seven systems comprise the standard L7 data set *(127)* and the C_{60}@[6]CPPA buckyball-in-a-ring complex is from Ref. *(131)*.

the two calculations *(131)*. As such, we will not compare DFT calculations directly to one of these benchmarks or the other, but will instead consider both benchmarks side-by-side.

We do this in Fig. 15, comparing both benchmarks (with estimated error bars) to a variety of DFT results. The latter do nothing to elucidate the nature of the discrepancy between the benchmarks, as the DFT values vary widely and do not seem to hew any more closely to one set of benchmarks as compared the other. Moreover, errors are much larger than the ~ 0.5 kcal/mol accuracy that has been documented for small, charge-neutral dimers. Whereas dispersion-inclusive DFT methods systematically (albeit slightly) overbind small dimers, as compared to CCSD(T)/CBS calculations, no such trend is observed for these larger systems and the errors seem equally likely to have either sign. This is more apparent from Fig. 16, which also includes baseline results for functionals that do not describe dispersion at all: B97, BLYP, PBE, PBE0, and B3LYP. As expected, the no-dispersion functionals systematically underbind these complexes, by ≥ 10 kcal/mol in every case except for the phenylalanine trimer that contains multiple hydrogen bonds. In other cases, these baseline functionals predict that the complex is unbound.

We next focus on two systems for which the FN-DMC and LNO-CCSD (T)/CBS benchmarks are statistically equivalent within error bars: adenine-on-circumcoronene (C3A) and the guanine–cytosine tetramer (GCGC). In both cases, we find that most of the dispersion-inclusive and dispersion-corrected DFT methods exhibit absolute errors larger than 1 kcal/mol. Many errors are larger than 2 kcal/mol and do not appear to skew towards over- or under-binding in any systematic way. This is interesting given the rather different nature of these two complexes, with hydrogen bonds present in GCGC that are absent in C3A. In the dispersion-dominated octadecane dimer and in the hydrogen-bonded phenylalanine trimer, for which the two benchmarks also agree within error bars, we find that most DFT methods overestimate the interaction energy for the former but mostly underestimate it for the latter. These errors are also larger than 1 kcal/mol. Of the larger complexes in Fig. 14, the only one for which the DFT errors are consistently smaller than 1 kcal/mol is the guanine trimer, but it has the smallest interaction energy at about 2 kcal/mol.

For C2C2PD, G3GC, and C_{60}@[6]CPPA there is not yet one unassailable benchmark because the difference between the FN-DMC and LNO-CCSD (T)/CBS interaction energies lies outside of the mutual error bars of either. Examination of DFT errors is informative, nevertheless. For C2C2PD, most

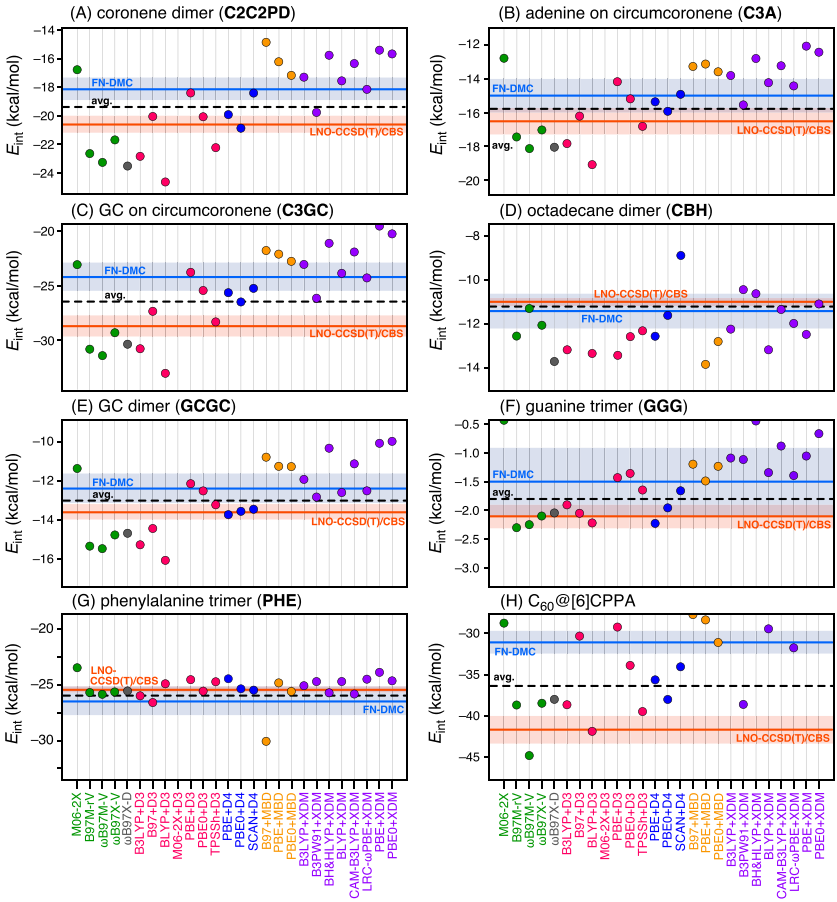

Fig. 15 DFT interaction energies for large vdW complexes, in comparison to LNO-CCSD(T)/CBS benchmarks (orange horizontal lines) and FN-DMC benchmarks (blue horizontal lines). Shaded regions in orange and blue indicate the uncertainty associated with either benchmark *(131)*, and dashed horizontal lines indicate the average of the two benchmarks. DFT calculations were performed using aug-cc-pVTZ for XDM and def2-QZVPD for other methods, except that def2-TZVPD was used for C_{60}@[6]CPPA. All DFT interaction energies are CP-corrected. Data points and functional names are color-coded according to the manner in which dispersion is described. Where certain DFT values are missing (for M06-2X+D3 and for several DFT+XDM methods applied to C_{60}@[6]CPPA), it means that E_{int} does not appear on the scale that is shown.

DFT methods afford errors larger than 1 kcal/mol, no matter which of the two benchmarks is used, and in many cases these errors are 3–4 kcal/mol. Errors range from 2–4 kcal/mol for C3GC, and for C_{60}@[6]CPPA they are

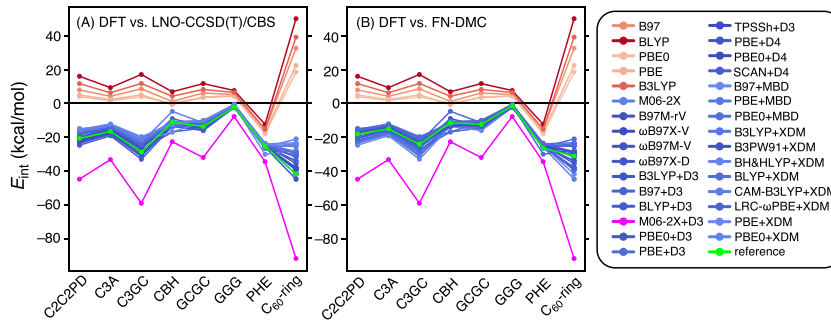

Fig. 16 DFT interaction energies for the systems in Fig. 14, as compared to reference values obtained from either (A) LNO-CCSD(T)/CBS or (B) FN-DMC calculations *(131)*. DFT calculations were performed using aug-cc-pVTZ for XDM and def2-QZVPD for other methods, except that def2-TZVPD was used for C_{60}@[6]CPPA. All DFT interaction energies are CP-corrected.

2–6 kcal/mol. As with cases for which the reference energy is more certain, DFT errors vary widely and there is no systematic trend toward over- or underestimation of the interaction energy.

The S12L data set *(55,94)* provides another set of large-system benchmarks, with reference energies that were originally extracted from solution-phase binding affinities (by subtracting estimated solvation energies and vibrational entropy corrections) *(94)*. Several of these complexes were later tackled using FN-DMC *(129)* and these are depicted in Fig. 17. More recently, CCSD(T)/CBS benchmarks became available *(134)*, using a domain-based localized pair natural orbital (DLPNO) approximation *(305–308)*. These benchmarks were obtained at the DLPNO-CCSD(T_0)/CBS level *(134)* where T_0 denotes a semicanonical triples correction *(306)*. Benchmarks were reported at the same level of theory for a ligand–protein complex consisting of indinavir bound to a model of HIV-II protease *(309)*, and for an intercalation complex of the anti-tumor agent ellipticine bound to double-stranded DNA *(310)*, for which a FN-DMC benchmark is also available *(311)*. The ellipticine@DNA and indinavir@HIV systems, which are also depicted in Fig. 17, have become standard noncovalent benchmark systems of pharmacological interest *(133,134,143,250,273,311–314)* The eight complexes in Fig. 17 are larger than the ones in Fig. 14 and range in size from 86 atoms (for the "tweezers" complex **2b**) *(315)* up to 323 atoms for indinavir@HIV. Due to their size, DFT calculations for these systems employ the def-TZVPD basis set, which should still lie close to the CBS limit once CP correction is applied *(88)*.

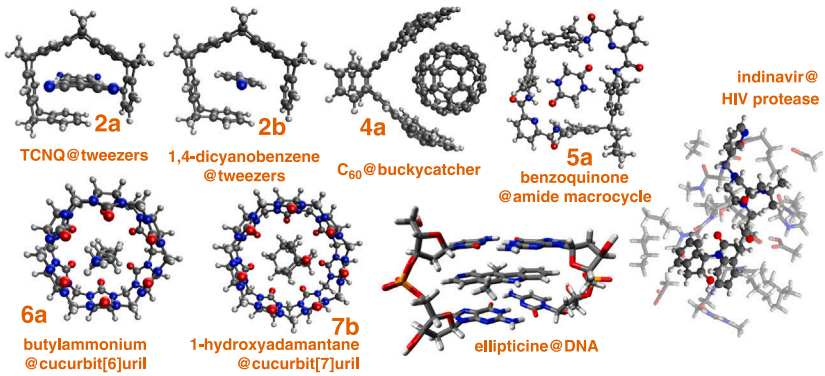

Fig. 17 Six of the 12 complexes in the S12L data set (**2a**, **2b**, **4a**, **5a**, **6a**, and **7b**) *(94)*, for which both FN-DMC *(129)* and DLPNO-CCSD(T_0)/CBS *(134)* benchmarks are available, along with an ellipticine@DNA intercalation complex and an indinavir@HIV ligand–protein complex.

Interaction energies for these complexes are plotted in Fig. 18. Once again, FN-DMC interaction energies are systematically less attractive than DLPNO-CCSD(T_0)/CBS values, with differences that lie outside of the mutual uncertainties in the putative benchmarks. Errors in the DLPNO approximation have been shown to be vanishingly small when tight thresholds are combined with extrapolation to the canonical limit *(301–304)*, even in sizable vdW complexes *(304)*, and the origin of the discrepancies with respect to FN-DMC remains unresolved.

DFT results for these systems fall into two categories. In one category are complexes **4a**, **7b**, and ellipticine@DNA, for which many of the DFT values lie between the two reference energies so there can be no consensus as to the sign of the DFT errors. On the other hand, for **2a**, **2b**, **5a**, and **6a** the DFT results are mostly characterized by systematic overbinding as compared to either benchmark, by up to 6.6 kcal/mol (BLYP+D3) for **2a**, 4.9 kcal/mol (ωB97X-D) for **2b**, or 8.3 kcal/mol (B97 +D3) for **6a**. (Quoted numerical errors reflect the DLPNO-CCSD(T_0)/CBS reference value.) The M06-2X functional, however, consistently performs very well and is within about 1 kcal/mol of DLPNO-CCSD(T_0)/CBS for all four of these complexes, although it performs poorly for **4a** (error = 14.1 kcal/mol) and **7b** (error = 7.4 kcal/mol). All functionals overbind the amide macrocycle complex **5a** *(316)*, by at least 3.5 kcal/mol with respect to the DLPNO-CCSD(T_0)/CBS reference. The indinavir@HIV complex is the largest system examined herein, with a benchmark $E_{\text{int}} = -121.50$ kcal/mol computed at the DLPNO-CCSD (T_0)/CBS level *(134)*. Some functionals come close to this although results

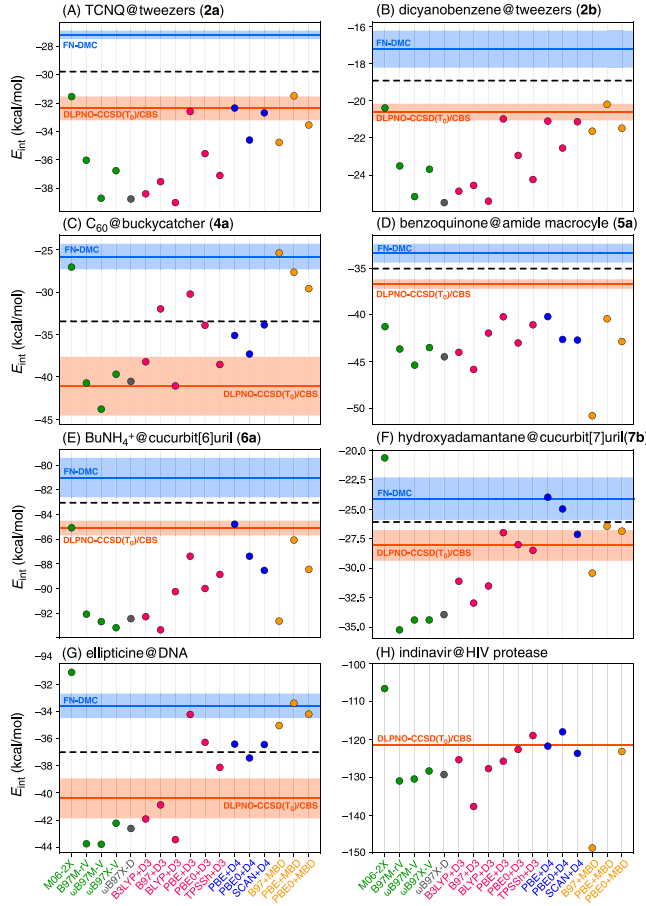

Fig. 18 CP-corrected DFT/def2-TZVPD interaction energies for the complexes in Fig. 17 compared to DLPNO-CCSD(T_0)/CBS reference values *(134)* (in orange) and FN-DMC reference values *(129,311)* (in blue). The dashed line represents the average of the two reference values and shaded regions indicate estimated uncertainties. A PBE+MBD value for indinavir@HIV was not computed due to SCF convergence problems.

overall are varied, with errors as large as 15 kcal/mol for M06-2X and 27 kcal/mol for B97+MBD.

The PBE+MBD interaction energy for indinavir@HIV is missing from Fig. 18 due to convergence problems that warrant discussion. Molecular electronic structure calculations using atom-centered Gaussian basis functions typically employ diagonalization-based SCF solvers rather than minimization-based solvers, as the former are generally more efficient when direct diagonalization is feasible. In our experience, however, this is

problematic for GGA calculations in large systems, especially in high-quality basis sets and in the presence of anionic functional groups. Ironically, we often find that a good way to converge a "low-cost" GGA calculation is to use a more expensive hybrid functional to generate a guess, as this tends to open up the HOMO/LUMO gap, but this trick did not work for PBE+MBD applied to indinavir@HIV. Severe convergence problems engendered by vanishing HOMO/LUMO gaps have also been noted when GGAs are applied to ionic liquids *(317)* and to proteins *(318–324)*. Some have suggested that these difficulties are artifacts of vacuum boundary conditions *(322,324)*, as convergence problems are often mitigated by means of dielectric boundary conditions *(322–326)*. (A classical point-charge environment may also help *(319,320,327)*). That said, hybrid functionals typically alleviate convergence problems *(317,320–322)*, even in the presence of vacuum boundary conditions, suggesting that GGAs are not altogether innocent in this regard. In our view, the issue is artificial charge delocalization due to self-interaction error, which is especially severe in systems containing anionic moieties *(326)*. Minimization-based solvers may avoid this problem by finding a local minimum that localizes charge *(328)*, whereas diagonalization-based solvers afford the (delocalized) global minimum, leading to charge sloshing during the SCF iterations that may hamper convergence.

In summary, DFT errors across nanoscale vdW complexes are highly varied, with few discernible systematic trends toward over- or under-binding behavior. This much can be stated even without resolving the issue of whether FN-DMC or local-orbital CCSD(T) provides the more reliable benchmark in the not-infrequent cases where the two disagree for large systems. However that question may ultimately be resolved, it is sobering to realize that DFT calculations in larger noncovalent systems do not afford the same level of accuracy that one can now expect from DFT for small vdW complexes. It is true that the interaction energies are simply larger in these larger systems, with $|E_{\text{int}}|$ ranging up to 42 kcal/mol for the systems in Fig. 14, according to LNO-CCSD(T)/CBS calculations *(131)*, and from 21–122 kcal/mol for the systems in Fig. 17, according to DLPNO-CCSD(T_0)/CBS calculations *(134)*. For comparison, the S66 interaction energies range up to $|E_{\text{int}}| = 19$ kcal/mol, but many of them are much smaller *(119)*. The largest systems considered here represent the present frontier for first-principles description of vdW interactions, where results with contemporary dispersion-aware DFT methods are promising but not yet quantitative.

4.2 Dispersion corrections

In (Fig. 19) we examine D3, D4, XDM, and MBD dispersion corrections for the L7 complexes, in comparison to SAPT+MBD values. The latter are taken to be benchmark dispersion energies, per the discussion in Section 3.1. As in smaller systems (Fig. 10), but at greatly expanded scale in these larger systems (Fig. 19), dispersion corrections for DFT are

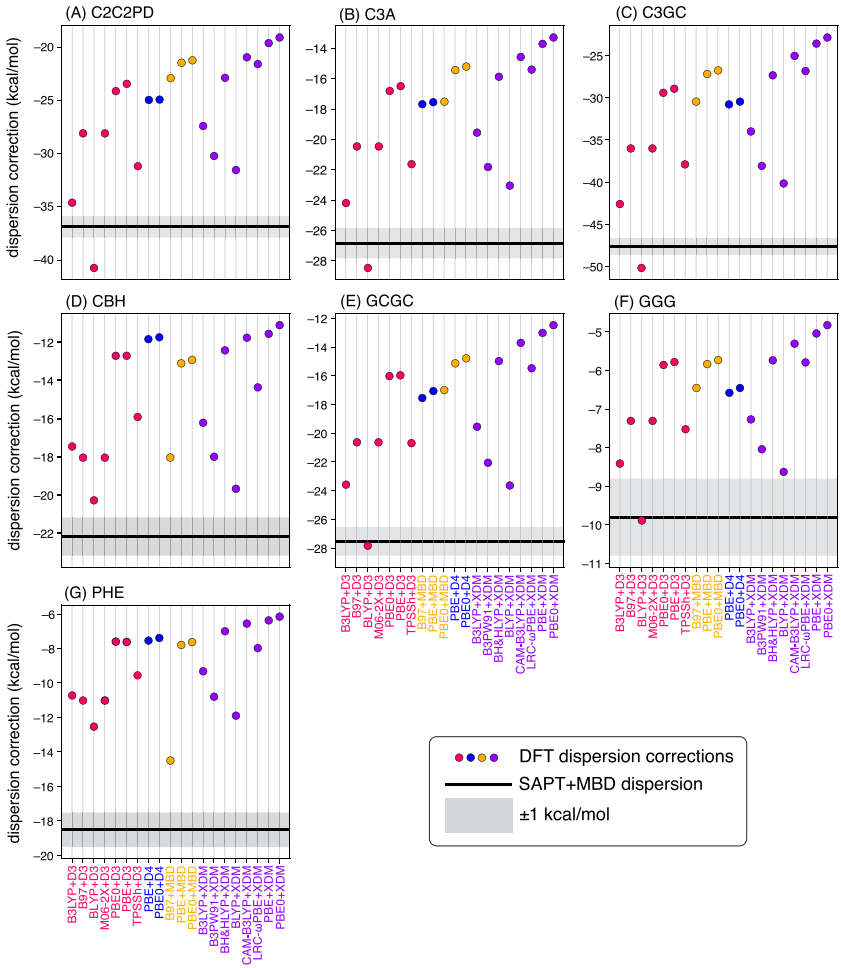

Fig. 19 Dispersion corrections (D3, D4, XDM, and MBD) for various density functionals, evaluated for the L7 data set and compared to SAPT+MBD/def2-SVPD benchmarks. The dispersion corrections for SCAN+D4 are not shown as they are too small to appear on this scale.

systematically smaller than true dispersion energies. This is expected, but the scale is noteworthy: more than 10 kcal/mol difference in some cases, underscoring that DFT dispersion corrections should not be equated with dispersion energies. Interestingly, BLYP+D3 is the lone functional (of those considered here) that bucks this trend, as its D3 correction is larger in magnitude than SAPT+MBD dispersion, in 5 of 7 cases, and is the largest among the DFT dispersion corrections in 6 of 7 cases. Other patterns emerge amongst the various dispersion-corrected methods, as seen from the very similar pattern of data points from one complex to the next, despite significant differences in the energy scale. The D4(BJ) correction for SCAN+D4 ranges from −2.5 to −23.1 kcal/mol for these systems and is off-scale in every case that appears in Fig. 19. This is notable given that SCAN+D4 performs reasonably well for the L7 complexes, with MAEs of 1.4 kcal/mol versus LNO-CCSD(T)/CBS or 0.9 kcal/mol versus FN-DMC. This suggests that a significant amount of middle-range dispersion is captured by the semilocal SCAN functional.

4.3 Counterpoise corrections

For interaction energies, larger system sizes equate to larger errors in DFT, even after accounting for uncertainty in the benchmarks. All of the large-system DFT calculations reported in this work were performed using basis sets no smaller than def2-TZVPD or aug-cc-pVTZ, and many of them use def2-QZVPD. Boys-Bernardi CP correction is used in every case. These interaction energies ought to lie close to the DFT/CBS limit *(88)*.

The magnitude of the BSSE grows with system size and in vdW complexes with $\gtrsim 100$ atoms, DFT/double-ζ interaction energies may err by 10–50 kcal/mol or more, simply due to BSSE, unless CP correction is applied; see Table 1. Additional large-system examples are provided in Fig. 20, illustrating how CP-corrected and uncorrected interaction energies converge to the CBS limit for large protein–ligand complexes *(88)*. Two of these examples involve small ligands (benzene and phenol) while two others contain larger ligands: 81 atoms for RU85052 and 92 atoms for indinavir. In all four cases, the protein model is large by quantum chemistry standards, up to 235 atoms, and these tests are part of ongoing efforts to obtain quantum-chemical results for enzymes that are converged with respect to the size of the model system *(326,329–331)*.

There is a tendency to avoid diffuse basis functions in large DFT calculations, as they dramatically increase the cost by hampering integral screening and may slow SCF convergence due to linear dependencies

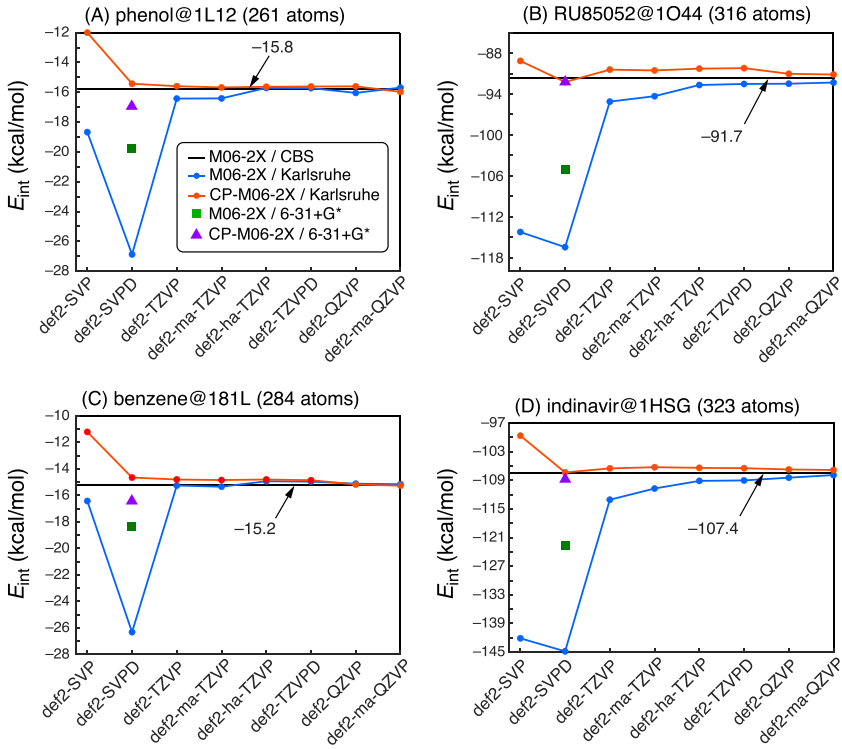

Fig. 20 Convergence to the M06-2X/CBS limit for interaction energies of large protein–ligand complexes, showing both CP-corrected and uncorrected results. The CBS limit, which is indicated by the horizontal black line and whose numerical value is provided in kcal/mol, is estimated using the average of CP-corrected and uncorrected M06-2X/def2-ma-QZVPD interaction energies. *Reproduced with permission from Gray, M.; Bowling, P. E.; Herbert, J. M. Systematic Evaluation of Counterpoise Correction in Density Functional Theory. J. Chem. Theory Comput.* ***2022,*** *18, 6742–6756; copyright 2022 American Chemical Society.*

unless very tight thresholds are used *(239)*. For the protein–phenol and protein–benzene complexes in Fig. 20A and 20B, calculations at the M06-2X/def2-SVP level engender ≈ 6 kcal/mol of BSSE, as measured by the magnitude of the CP correction, but for the indinavir@1HSG complex in (Fig. 20D) that difference is more than 40 kcal/mol! These differences persist even when diffuse functions are added, yet a single set of diffuse functions in combination with CP correction significantly improves each of the ligand–protein interaction energies in Fig. 20. M06-2X(CP)/def2-SVPD results are within 1 kcal/mol of M06-2X/CBS values. In the absence of CP correction, that level of convergence is not reached for the

large-ligand systems unless the def2-TZVPD basis set is used. As such, CP correction should be considered mandatory in all noncovalent calculations that use Gaussian basis sets.

5. The future of noncovalent DFT

In part, this chapter serves to document how far DFT has evolved in its description of noncovalent interactions, as compared to early days of unbound rare-gas dimers and convoluted discussions of which (ultimately inappropriate) semilocal XC functional should be used for weak interactions *(332,333)*. For small noncovalent dimers, sub-kcal/mol accuracy is now achievable by means of a wide variety of different functionals, some of which include dispersion effects natively while others are explicitly dispersion-corrected. These dispersion corrections cannot and should not be equated to true dispersion energies, because the *ad hoc* correction is intermingled with semilocal XC effects at typical vdW contact distances, yet there are clear correlations with respect to genuine dispersion energies. Interpretative issues aside, the performance of DFT+D3, DFT+D4, DFT+XDM, and DFT+MBD is extremely promising and in small systems the accuracy of these methods is also rather similar. This is hardly surprising given the common physical underpinnings of each model, in the form of the Casimir-Polder relation between atomic polarizabilities and pairwise C_6 coefficients Eq. (6).

The "small" systems considered here have up to ~ 20 heavy atoms, which is certainly not a hard limit on good performance but represents the largest dimers in standard small-molecule data sets such as S22 and S66, for which DFT methods have been exhaustively vetted. Significantly larger systems with $\gtrsim 100$ atoms pose both a challenge and a conundrum. The quality of the reference data can be difficult to assess for systems of this size *(176)*, and indeed the best-available *ab initio* benchmarks for nanoscale vdW complexes differ from one another in a few noteworthy cases *(131,134)*. Nevertheless, the analysis presented herein makes it clear that the sub-kcal/mol accuracy of dispersion-aware DFT does not extend to systems of this size, uncertainties in the benchmarks notwithstanding. For the largest systems examined here (containing up to 323 atoms), DFT errors exceed 4 kcal/mol in many cases, with considerable variation amongst different methods, even when the comparison set is limited to methods that perform very well for small noncovalent dimers. BSSE can be very large in systems of this size ($\sim$50 kcal/mol

or more in double-ζ basis sets) *(88)*, although this is handled rather easily with the standard Boys-Bernardi CP scheme, avoiding the need for triple-ζ basis sets in large systems. There has sometimes been an odd resistance to using CP correction, as detailed elsewhere *(88)*, but benchmark assessments provide no support for such recalcitrance.

Nanoscale vdW complexes represent the current frontier in the continuing development of DFT for noncovalent interactions. Large variations amongst the best-performing methods suggest that new functionals may be required, fto improve upon the pairwise-additive foundation of the VV10 functional *(16)*, for example. Experimental data for gas-phase conformational energies in systems with $\gtrsim 150$ atoms are starting to become available *(136–138)*, and these make for much cleaner benchmarks as compared to solution-phase data where solvation modeling is a major source of error *(140,334)*. Based on these emerging experiments, it is suggested that existing DFT methods may overstabilize compact molecular conformations, relative to experiment *(136)*. Calorimetry measurements in medium-sized organic molecules can also be used to make contact with noncovalent interactions *(335)*, shedding light on the interplay between steric effects and dispersion in large molecules, or what has been called "steric attraction" *(99,100)*. These efforts should be further pursued in order to extend the threshold system size below which one may confidently state that nonbonded interactions are a solved problem in modern quantum chemistry.

Notes

New XDM damping parameters R_{ab}^{vdW} [Eq. (4)] were added to Q-Chem v. 6.1.1 as part of this work, based on an implementation of the XDM model by Kong et al. *(338)*. These parameters were taken from Otero-de-la-Roza and Johnson *(211)*.

Acknowledgements

This work was supported by the U.S. Department of Energy, Office of Basic Energy Sciences, Division of Chemical Sciences, Geosciences, and Biosciences under Award No. DE-SC0008550. Some calculations were performed at the Ohio Supercomputer Center *(336)*, using Q-Chem v. 6.1.1 *(337)*.

Conflict of interest

J.M.H. is part owner of Q-Chem and serves on its board of directors.

References

1. Patton, D. C.; Pederson, M. R. A Theoretical Study of Rare-Gas Diatomic Molecules with the Generalized-Gradient Approximation to Density Functional Theory. *Int. J. Quantum Chem.* **1998,** *69*, 619–627.
2. Kurita, N.; Sekino, H. *Ab Initio* and DFT Studies for Accurate Description of van Der Waals Interaction Between Rare-Gas Atoms. *Int. J. Quantum Chem.* **2003,** *91*, 355–362.
3. Fritsche, L.; Koller, J.; Reinert, T. Borderline Cases in Density Functional Theory. *Int. J. Quantum Chem.* **2004,** *100*, 681–694.
4. Proynov, E. I.; Ruiz, E.; Vela, A. et al. Determining and Extending the Domain of Exchange and Correlation Functionals. *Int. J. Quantum Chem. Symp* **1995,** *29*, 61–78.
5. Lundqvist, B. I.; Andersson, Y.; Shao, H. et al. Density Functional Theory Including van der Waals Forces. *Int. J. Quantum Chem.* **1995,** *56*, 247–255.
6. Lein, M.; Dobson, J. F.; Gross, E. K. U. Toward the Description of van der Waals Interactions Within Density Functional Theory. *J. Comput. Chem.* **1999,** *20*, 12–22.
7. Heßelmann, A.; Jansen, G. Intermolecular Dispersion Energies from Time-Dependent Density Functional Theory. *Chem. Phys. Lett.* **2003,** *367*, 778–784.
8. Misquitta, A. J.; Jeziorski, B.; Szalewicz, K. Dispersion Energy from Density-Functional Theory Description of Monomers. *Phys. Rev. Lett.* **2003,** *91*, 033201.
9. Dobson, J. F.; Dinte, B. P. Constraint Satisfaction in Local and Gradient Susceptibility Approximations: Application to a van der Waals Density Functional. *Phys. Rev. Lett.* **1996,** *76*, 1780–1783.
10. Dobson, J. Prospects for a van der Waals Density Functional. *Int. J. Quantum Chem.* **1998,** *69*, 615–618.
11. Dobson, J. F.; Dinte, B. P.; Wang, J. Van der Waals Functionals via Local Approximations for Susceptibilities. In *Electronic Density Functional Theory: Recent Progress and New Directions;* Dobson, J. F., Vignale, G., Das, M. P., Eds.; Springer Science+Business Media: New York, 1998.
12. Andersson, Y.; Langreth, D. C.; Lundqvist, B. I. Van der Waals Interactions in Density-Functional Theory. *Phys. Rev. Lett.* **1999,** *76*, 102–105.
13. Andersson, Y.; Hult, E.; Rydberg, H. et al. Van der Waals Interactions in Density Functional Theory. In *Electronic Density Functional Theory: Recent Progress and New Directions;* Dobson, G., Vignale, M. P., Eds.; Springer Science+Business Media: Boston, 1998.
14. Rydberg, H.; Lundqvist, B. I.; Langreth, D. C. et al. Tractable Nonlocal Correlation Density Functionals for Flat Surfaces and Slabs. *Phys. Rev. B* **2000,** *62*, 6997–7006.
15. Langreth, D. C.; Dion, M.; Rydberg, H. et al. Van der Waals Density Functional Theory with Applications. *Int. J. Quantum Chem.* **2005,** *101*, 599–610.
16. Calbo, J.; Ortí, J.; Sancho-García, J. C. et al. The Nonlocal Correlation Density Function VV10: A Successful Attempt to Accurately Capture Noncovalent Interactions.*Annu. Rep. Comput. Chem.* **2015,** *11*, 37–102.
17. Dion, M.; Rydberg, H.; Schröder, E. et al. Van der Waals Density Functional for General Geometries. *Phys. Rev. Lett.* **2004,** *92*, 246401. Erratum: Phys. Rev. Lett. 2005, 92, 109902.
18. Langreth, D. C.; Lundqvist, B. I.; Chakarova-Käck, S. D. et al. A Density Functional for Sparse Matter. *J. Phys.: Condens. Matt* **2009,** *21*, 084203.
19. Lee, K.; Murray, É. D.; Kong, L. et al. Higher-Accuracy Van Der Waals Density Functional. *Phys. Rev. B* **2010,** *82*, 081101.
20. Schröder, E.; Cooper, V. R.; Berland, K. et al. The vdW-DF Family of Nonlocal Exchange-Correlation Functionals. In *Non-Covalent Interactions in Quantum Chemistry and Physics;* de la Roza, A. O., DiLabio, G. A., Eds.; Elsevier: Amsterdam, 2017; pp. 241–274. Chapter 8.

21. Vydrov, O. A.; Van Voorhis, T. Improving the Accuracy of the Nonlocal van der Waals Density Functional with Minimal Empiricism. *J. Chem. Phys.* **2009,** *130*, 104105.
22. Vydrov, O. A.; Van Voorhis, T. Nonlocal van der Waals Density Functional Theory Made Simple. *Phys. Rev. Lett.* **2009,** *103*, 063004.
23. Vydrov, O. A.; Van Voorhis, T. Nonlocal van der Waals Density Functional: The Simpler the Better. *J. Chem. Phys.* **2010,** *133*, 244103.
24. Vydrov, O. A.; Van Voorhis, T. Nonlocal van der Waals Density Functionals Based on Local Response Models. In *Fundamentals of Time-Dependent Density Functional Theory, vol. 837;* Marques, M. A. L., Maitra, N. T., Nogueira, F. M. S., Eds.; Springer-Verlag: Berlin, 2012; pp. 443–456. Chapter 23.
25. Mardirossian, N.; Head-Gordon, M. ωB97X-V: A 10-Parameter, Range-Separated Hybrid, Generalized Gradient Approximation Density Functional with Nonlocal Correlation, Designed by a Survival-of-the-Fittest Strategy. *Phys. Chem. Chem. Phys.* **2014,** *16*, 9904–9924.
26. Mardirossian, N.; Head-Gordon, M. ω B97M-V: A Combinatorially Optimized, Range-Separated Hybrid, Meta-GGA Density Functional with VV10 Nonlocal Correlation. *J. Chem. Phys.* **2016,** *144*, 214110.
27. Mardirossian, N.; Head-Gordon, M. Mapping the Genome of Meta-Generalized Gradient Approximation Density Functionals: The Search for B97M-V. *J. Chem. Phys.* **2015,** *142*, 074111.
28. Mardirossian, N.; Pestana, L. R.; Womack J. C. et al. Use of the rVV10 Nonlocal Correlation Functional in the B97M-V Density Functional: Defining B97M-rV and Related Functionals.*J. Phys. Chem. Lett.* **2017,** *8*, 35–40.
29. Mardirossian, N.; Head-Gordon, M. Survival of the Most Transferable at the Top of Jacob's Ladder: Defining and Testing the ωB97M(2) Double Hybrid Density Functional. *J. Phys. Chem.* **2018,** *148*, 241736.
30. Mardirossian, N.; Head-Gordon, M. Thirty Years of Density Functional Theory in Computational Chemistry: An Overview and Extensive Assessment of 200 Density Functionals. *Mol. Phys.* **2017,** *115*, 2315–2372.
31. Grimme, S.; Hansen, A.; Brandenburg, J. G. et al. Dispersion-Corrected Mean-Field Electronic Structure Methods. *Chem. Rev.* **2016,** *116*, 5105–5154.
32. Hermann, J.; DiStasio; Tkatchenko, A. First-Principles Models for van der Waals Interactions in Molecules and Materials: Concepts, Theory, and Applications. *Chem. Rev.* **2017,** *117*, 4714–4758.
33. Stöhr, M.; Van Voorhis, T.; Tkatchenko, A. Theory and Practice of Modeling van der Waals Interactions in Electronic-Structure Calculations. *Chem. Soc. Rev.* **2019,** *48*, 4118–4154.
34. Grimme, S. Density Functional Theory with London Dispersion Corrections. *Wiley Interdiscip. Rev.:Comput. Mol. Sci* **2011,** *1*, 211–228.
35. Grimme, S. Semiempirical GGA-Type Density Functional Constructed with a Long-Range Dispersion Correction. *J. Comput. Chem.* **2006,** *27*, 1787–1799.
36. Grimme, S.; Antony, J.; Ehrlich, S. et al. A Consistent and Accurate *ab Initio* Parameterization of Density Functional Dispersion Correction (DFT-D) for the 94 Elements H–Pu. *J. Chem. Phys.* **2010,** *132*, 154104.
37. Caldeweyher, E.; Bannwarth, C.; Grimme, S. Extension of the D3 Dispersion Coefficient Model. *J. Chem. Phys.* **2017,** *147*, 034112.
38. Otero-de-la-Roza, A.; LeBlanc, L. M.; Johnson, E. R. What Is "Many-body" Dispersion and Should I Worry About It?*Phys. Chem. Chem. Phys.* **2020,** *22*, 8266–8276.
39. Conway, A.; Murrell, J. N. The Exchange Energy Between Two Neon Atoms. *Mol. Phys.* **1974,** *27*, 873–878.

40. Cohen, J. S.; Pack, R. T. Modified Statistical Method for Intermolecular Potentials. Combining Rules for Higher van der Waals Coefficients. *J. Chem. Phys.* **1974,** *61*, 2372–2382.
41. Hepburn, J.; Scoles, G.; Penco, R. A Simple but Reliable Method for the Prediction of Intermolecular Potentials. *Chem. Phys. Lett.* **1975,** *36*, 451–456.
42. Ahlrichs, R.; Penco, R.; Scoles, G. Intermolecular Forces in Simple Systems. *Chem. Phys.* **1977,** *19*, 119–130.
43. Hobza, P.; Zahradník, R. Van der Waals Molecules: Quantum Chemistry, Physical Properties, and Reactivity. *Int. J. Quantum Chem.* **1983,** *23*, 325–338.
44. Becke, A. D.; Johnson, E. R. Exchange-Hole Dipole Moment and the Dispersion Interaction. *J. Chem. Phys.* **2005,** *122*, 154104.
45. Johnson, E. R.; Becke, A. D. A Post-Hartree–Fock Model of Intermolecular Interactions. *J. Chem. Phys.* **2005,** *123*, 024101.
46. Johnson, E. R.; Becke, A. D. A Post-Hartree–Fock Model of Intermolecular Interactions: Inclusion of Higher-Order Corrections. *J. Chem. Phys.* **2006,** *124*, 174104.
47. Becke, A. D.; Johnson, E. R. A Density-Functional Model of the Dispersion Interaction. *J. Chem. Phys.* **2005,** *123*, 154101.
48. Becke, A. D.; Johnson, E. R. Exchange-Hole Dipole Moment and the Dispersion Interaction: High-Order Dispersion Coefficients. *J. Chem. Phys.* **2006,** *124*, 014104.
49. Becke, A. D.; Johnson, E. R. Exchange-Hole Dipole Moment and the Dispersion Interaction Revisited. *J. Chem. Phys.* **2007,** *127*, 154108.
50. Johnson, E. R. The Exchange-Hole Dipole Moment Dispersion Model. In *Non-Covalent Interactions in Quantum Chemistry and Physics*; de la Roza, A. O.; DiLabio, G. A., Eds.; Elsevier: Amsterdam, 2017; pp. 169–194 Chapter 5.
51. Tkatchenko, A.; Scheffler, M. Accurate Molecular van der Waals Interactions from Ground-State Electron Density and Free-Atom Reference Data. *Phys. Rev. Lett.* **2009,** *102*, 073005.
52. Al-Saidi, W. A.; Voora, V. K.; Jordan, K. D. An Assessment of the vdW-TS Method for Extended Systems. *J. Chem. Theory Comput.* **2012,** *8*, 1503–1513.
53. Dobson, J. F. Beyond Pairwise Additivity in London Dispersion Interactions. *Int. J. Quantum Chem.* **2014,** *114*, 1157–1161.
54. von Lilienfeld, O. A.; Tkatchenko, A. Two- and Three-Body Interatomic Dispersion Energy Contributions to Binding in Molecules and Solids. *J. Chem. Phys.* **2010,** *132*, 234109.
55. Risthaus, T.; Grimme, S. Benchmarking of London Dispersion-Accounting Density Functional Theory Methods on Very Large Molecular Complexes. *J. Chem. Theory Comput.* **2013,** *9*, 1580–1591.
56. Lao, K. U.; Herbert, J. M. Atomic Orbital Implementation of Extended Symmetry-Adapted Perturbation Theory (XSAPT) and Benchmark Calculations for Large Supramolecular Complexes. *J. Chem. Theory Comput.* **2018,** *14*, 2955–2978.
57. Proynov, E.; Liu, F.; Gan, Z., et al. Density-Functional Approach to the Three-Body Dispersion Interaction Based on the Exchange Dipole Moment. *J. Chem. Phys.* **2015,** *143*, 084125.
58. Axilrod, B. M.; Teller, E. Interaction of the van der Waals Type Between Three Atoms. *J. Chem. Phys.* **1943,** *11*, 299–301.
59. Muto, Y. Forces Between Nonpolar Molecules. *J. Phys. -Math. Soc. Japan* **1943,** *17*, 629.
60. Tkatchenko, A.; DiStasio; Car, R. et al. Accurate and Efficient Method for Many-Body van der Waals Interactions. *Phys. Rev. Lett.* **2012,** *108*, 236402.

61. Ambrosetti, A.; Reilly, A. M.; DiStasio, Jr., R. A., et al. Long-Range Correlation Energy Calculated from Coupled Atomic Response Functions. *J. Chem. Phys.* **2014,** *140*, 18A508.
62. Hermann, J.; Tkatchenko, A. Density Functional Model for van der Waals Interactions: Unifying Many-Body Atomic Approaches with Nonlocal Functionals. *Phys. Rev. Lett.* **2020,** *124*, 146401.
63. Góger, S.; Khabibrakhmanov, A.; Vaccarelli, O. et al. Optimized Quantum Drude Oscillators for Atomic and Molecular Response Properties. *J. Phys. Chem. Lett.* **2023,** *14*, 6217–6223.
64. Price, A. J. A.; Bryenton, K. R.; Johnson, E. R. Requirements for an Accurate Dispersion-Corrected Density Functional. *J. Chem. Phys.* **2021,** *154*, 230902.
65. Hermann, J.; Tkatchenko, A. Electronic Exchange and Correlation in van der Waals Systems: Balancing Semilocal and Nonlocal Energy Contributions. *J. Chem. Theory Comput.* **2018,** *14*, 1361–1369.
66. Sherrill, C. D.; Takatani, T.; Hohenstein, E. G. An Assessment of Theoretical Methods for Nonbonded Interactions: Comparison to Complete Basis Set Limit Coupled-Cluster Potential Energy Curves for Benzene Dimer, the Methane Dimer, Benzene-Methane, and Benzene-H_2S. *J. Phys. Chem. A* **2009,** *113*, 10146–10159.
67. Sinnokrot, M. O.; Sherrill, C. D. Highly Accurate Coupled Cluster Potential Energy Curves for the Benzene Dimer: Sandwich, T-Shaped, and Parallel-Displaced Configurations. *J. Phys. Chem. A* **2004,** *108*, 10200–10207.
68. Sinnokrot, M. O.; Sherrill, C. D. High-Accuracy Quantum Mechanical Studies of π–π Interactions in Benzene Dimers. *J. Phys. Chem. A* **2006,** *110*, 10656–10668.
69. Carter-Fenk, K.; Herbert, J. M. Electrostatics Does Not Dictate the Slip-Stacked Arrangement of Aromatic π –π Interactions. *Chem. Sci* **2020,** *11*, 6758–6765.
70. Carter-Fenk, K.; Herbert, J. M. Reinterpreting π -Stacking. *Phys. Chem. Chem. Phys.* **2020,** *22*, 24870–24886.
71. Perdew, J. P.; Burke, K.; Ernzerhof, M. Generalized Gradient Approximations Made Simple. *Phys. Rev. Lett.* **1996,** 77, 3865–3868. Erratum: Phys. Rev. Lett. 1997, 78, 1396.
72. Patkowski, K. Benchmark Databases of Intermolecular Interaction Energies: Design, Construction, and Significance. *Annu. Rep. Comput. Chem.* **2017,** *13*, 3–91.
73. Becke, A. D. Density-Functional Thermochemistry. III. The Role of Exact Exchange. *J. Chem. Phys.* **1993,** *98*, 5648–5652.
74. Lee, C.; Yang, W.; Parr, R. G. Development of the Colle-Salvetti Correlation-Energy Formula into a Functional of the Electron Density. *Phys. Rev. B* **1988,** *37*, 785–789.
75. Zhao, Y.; Truhlar, D. G. The M06 Suite of Density Functionals for Main Group Thermochemistry, Thermochemical Kinetics, Noncovalent Interactions, Excited States, and Transition Elements: Two New Functionals and Systematic Testing of Four M06-Class Functionals and 12 Other Functionals. *Theor. Chem. Acc.* **2008,** *120*, 215–241. Erratum: Theor. Chem. Acc. 2008, 119, 525.
76. Perdew, J. P.; Schmidt, K. Jacob's Ladder of Density Functional Approximations for the Exchange-Correlation Energy. *AIP Conf. Proc* **2001,** *577*, 1–20.
77. Perdew, J. P.; Ruzsinszky, A.; Tao, J. et al. Prescription for the Design and Selection of Density Functional Approximations: More Constraint Satisfaction with Fewer Fits. *J. Chem. Phys.* **2005,** *123*, 062201.
78. Herbert, J. M. Density-Functional Theory for Electronic Excited States. In *Theoretical and Computational Photochemistry: Fundamentals, Methods, Applications and Synergy with Experimental Approaches;* García-Iriepa, C., Marazzi, M., Eds.; Elsevier: Amsterdam, 2023; pp. 69–118. Chapter 3.

79. Becke, A. D. A New Mixing of Hartree–Fock and Local Density-Functional Theories. *J. Chem. Phys.* **1993,** *98*, 1372–1377.
80. Bauschlicher, Jr., C. W.; Partridge, H. The Sensitivity of B3LYP Atomization Energies to the Basis Set and a Comparison of Basis Set Requirements for CCSD(T) and B3LYP. *Chem. Phys. Lett.* **1995,** *240*, 533–540. Erratum: Chem. Phys. Lett. 1998, 287, 216.
81. Frisch, M. J.; Trucks, G. W.; Cheeseman, J. R. Systematic Model Chemistries Based on Density Functional Theory: Comparison with Traditional Models and with Experiment. In *Recent Developments and Applications of Modern Density Functional Theory;* Seminario J. M., Ed.; Elsevier: Amsterdam, 1996; pp. 679–707.
82. Martell, J. M.; Goddard, J. D.; Eriksson, L. A. Assessment of Basis Set and Functional Dependencies in Density Functional Theory: Studies of Atomization and Reaction Energies. *J. Phys. Chem. A* **1997,** *101*, 1927–1934.
83. Jurečka, P.; Černý, J.; Hobza, P. et al. Density Functional Theory Augmented with an Empirical Dispersion Term. Interaction Energies and Geometries of 80 Noncovalent Complexes Compared with *ab Initio* Quantum Mechanics Calculations. *J. Comput. Chem* **2006,** *28*, 555–569.
84. Burns, L. A.; Vázquez-Mayagoitia, A.; Sumpter, B. G. et al. Density-Functional Approaches to Noncovalent Interactions: A Comparison of Dispersion Corrections (DFT-D), Exchange-Hole Dipole Moment (XDM) Theory, and Specialized Functionals. *J. Chem. Phys.* **2011,** *134*, 084107.
85. Goerigk, L.; Kruse, H.; Grimme, S. Benchmarking Density Functional Methods Against the S66 and S66×8 Datasets for Non-Covalent Interactions. *ChemPhysChem* **2011,** *12*, 3421–3433.
86. Marom, N.; Tkatchenko, A.; Rossi, M. et al. Dispersion Interactions with Density-Functional Theory: Benchmarking Semiempirical and Interatomic Pairwise Corrected Density Functionals. *J. Chem. Theory Comput.* **2011,** *7*, 3944–3951.
87. Goerigk, L.; Grimme, G. A Thorough Benchmark of Density Functional Methods for General Main Group Thermochemistry, Kinetics, and Noncovalent Interactions. *Phys. Chem. Chem. Phys.* **2011,** *13*, 6670–6688.
88. Gray, M.; Bowling, P. E.; Herbert, J. M. Systematic Examination of Counterpoise Correction in Density Functional Theory. *J. Chem. Theory Comput.* **2022,** *18*, 6742–6756.
89. Dasgupta, S.; Palos, E.; Pan, Y. et al. Balance Between Physical Interpretability and Energetic Predictability in Widely Used Dispersion-Corrected Density Functionals. *J. Chem. Theory Comput.* **2024,** *20*, 49–67.
90. Gruzman, D.; Karton, A.; Martin, J. M. L. Performance of *ab Initio* and Density Functional Methods for Conformational Equilibria of C_n H_{2n+2} Alkane Isomers (n = 4–8). *J. Phys. Chem. A* **2009,** *113*, 11974–11983.
91. Huenerbein, R.; Schirmer, B.; Moellmann, J. et al. Effects of London Dispersion on the Isomerization Reactions of Large Organic Molecules: A Density Functional Benchmark Study. *Phys. Chem. Chem. Phys.* **2010,** *12*, 6940–6948.
92. Ehlert, S.; Grimme, S.; Hansen, A. Conformational Energy Benchmark for Longer *n*-Alkane Chains. *J. Phys. Chem. A* **2022,** *126*, 3521–3535.
93. Sirianni, D. A.; Alenaizan, A.; Cheney, D. L. et al. Assessment of Density Functional Methods for Geometry Optimization of Bimolecular van der Waals Complexes. *J. Chem. Theory Comput.* **2018,** *14*, 3004–3013.
94. Grimme, S. Supramolecular Binding Thermodynamics by Dispersion-Corrected Density Functional Theory. *Chem. Eur. J* **2012,** *18*, 9955–9964.
95. Grimme, S. Dispersion Interaction and Chemical Bonding. In *The Chemical Bond: Chemical Bonding across the Periodic Table;* Frenking, G., Shaik, S., Eds.; Wiley-VCH: Weinheim, 2014; pp. 477–499. Chapter 16.

96. Řezáč, J.; Bím, D.; Gutten, O. et al. Toward Accurate Conformational Energies of Smaller Peptides and Medium-Sized Macrocycles: MPCONF196 Benchmark Energy Data Set. *J. Chem. Theory Comput.* **2018,** *14*, 1254–1266.
97. Scümann, J. M.; Wagner, J. P.; Eckhardt, A. K. et al. Intramolecular London Dispersion Interactions Do Not Cancel in Solution. *J. Am. Chem. Soc.* **2021,** *143*, 41–45.
98. Wagner, J. P.; Schreiner, P. R. London Dispersion in Molecular Chemistry—Reconsidering Steric Effects. *Angew Chem. Int. Ed. Engl.* **2015,** *54*, 12274–12279.
99. Gryn'ova, G.; Corminboeuf, C. Steric "Attraction": Not by Dispersion Alone. *Beilstein J. Org. Chem.* **2018,** *14*, 1482–1490.
100. Holtrop, F.; Visscher, K. W.; Jupp, A. R. et al. Steric Attraction: A Force to Be Reckoned with. *Adv. Phys. Org. Chem* **2020,** *54*, 119–141.
101. Solel, E.; Ruth, M.; Schreiner, P. R. London Dispersion Helps Refine Steric A-Values: Dispersion Energy Donor Scales. *J. Am. Chem. Soc.* **2021,** *143*, 20837–20848.
102. Rummel, L.; Domanski, M. H. J.; Hausmann, H. et al. London Dispersion Favors Sterically Hindered Diarylthiourea Conformers in Solution. *Angew. Chem. Int. Ed. Engl.* **2022,** *61*, e202204393.
103. Bursch, M.; Grimme, S.; Hansen, A. Influence of Steric and Dispersion Interactions on the Thermochemistry of Crowded (Fluoro) Alkyl Compounds. *Acc. Chem. Res.* **2024,** *57*, 153–163.
104. Lin, I.-C.; Seitsonen, A. P.; Coutinho-Neto, M. D. et al. Importance of van der Waals Interactions in Liquid Water. *J. Phys. Chem. B* **2009,** *113*, 1127–1131.
105. Lin, I.-C.; Seitsonen, A. P.; Tavernelli, I. et al. Structure and Dynamics of Liquid Water from *ab Initio* Molecular Dynamics—Comparison of BLYP, PBE, and revPBE Density Functionals with and Without van der Waals Corrections. *J. Chem. Theory Comput.* **2012**, 8.
106. Jones, A.; Cipcigan, F.; Sokhan, V. P. et al. Electronically Coarse-Grained Model for Water. *Phys. Rev. Lett.* **2013,** *110*, 227801.
107. Sokhan, V. P.; Jones, A. P.; Cipcigan, F. S. et al. Signature Properties of Water: Their Molecular Electronic Origins. *Proc. Natl. Acad. Sci. USA* **2015,** *112*, 6341–6346.
108. Gillan, M. J.; Alfè, D.; Michaelides, A. Perspective: How Good Is DFT for Water?*J. Chem. Phys.* **2016,** *144*, 130901.
109. Perlt, E.; Ray, P.; Hansen, A. et al. Finding the Best Density Functional Approximation to Describe Interaction Energies and Structures of Ionic Liquids in Molecular Dynamics Studies. *J. Chem. Phys.* **2018,** *148*, 193835.
110. Otero-de-la-Roza, A.; Johnson, E. R. A Benchmark for Non-Covalent Interactions in Solids. *J. Chem. Phys.* **2012,** *137*, 054103.
111. Santra, B.; Klimeš, J.; Alfè, D. et al. Hydrogen Bonds and van der Waals Forces in Ice at Ambient and High Pressures. *Phys. Rev. Lett.* **2011,** *107*, 185701.
112. Santra, B.; Klimeš, J.; Tkatchenko, A. et al. On the Accuracy of van der Waals Inclusive Density-Functional Theory Exchange-Correlation Functionals for Ice at Ambient and High Pressures. *J. Chem. Phys.* **2013,** *139*, 154702.
113. Kronik, L.; Tkatchenko, A. Understanding Molecular Crystals with Dispersion-Inclusive Density Functional Theory: Pairwise Corrections and Beyond. *Acc. Chem. Res.* **2014,** *47*, 3208–3216.
114. Tawfik, S. A.; Gould, T.; Stampfl, C. et al. Evaluation of van der Waals Density Functionals for Layered Materials. *Phys. Rev. Mater* **2018,** *2*, 034005.
115. Otero-de-la-Roza, A.; LeBlanc, L. M.; Johnson, E. R. Asymptotic Pairwise Dispersion Corrections Can Describe Layered Materials Accurately. *J. Phys. Chem. Lett.* **2020,** *11*, 2298–2302.
116. Adeleke, A. A.; Johnson, E. R. Effects of Dispersion Corrections on the Theoretical Description of Bulk Metals. *Phys. Rev. B* **2023,** *107*, 064101.

117. Jurečka, P.; Šponer, J.; Černý, J. et al. Benchmark Database of Accurate (MP2 and CCSD(T) Complete Basis Set Limit) Interaction Energies of Small Model Complexes, DNA Base Pairs, and Amino Acid Pairs. *Phys. Chem. Chem. Phys.* **2006,** *8*, 1985–1993.
118. Takatani, T.; Hohenstein, E. G.; Malagoli, M. et al. Basis Set Consistent Revision of the S22 Test Set of Noncovalent Interaction Energies. *J. Chem. Phys.* **2010,** *132*, 144104.
119. Řezáč, J.; Riley, K. E.; Hobza, P. S66: A Well-Balanced Database of Benchmark Interaction Energies Relevant To Biomolecular Structures. *J. Chem. Theory Comput.* **2011,** 7, 2427–2438. Erratum: J. Chem. Theory Comput. 2014, 10, 1359–1360.
120. Řezáč, J.; Riley, K. E.; Hobza, P. Extensions of the S66 Data Set: More Accurate Interaction Energies and Angular-Displaced Nonequilibrium Geometries. *J. Chem. Theory Comput.* **2011,** 7, 3466–3470.
121. Řezáč, J.; Riley, K. E.; Hobza, P. Benchmark Calculations of Noncovalent Interactions of Halogenated Molecules. *J. Chem. Theory Comput.* **2012,** *8*, 4285–4292.
122. Řezáč, J.; Hobza, P. Describing Noncovalent Interactions Beyond the Common Approximations: How Accurate Is the "Gold Standard", CCSD(T) at the Complete Basis Set Limit?*J. Chem. Theory Comput.* **2013,** *9*, 2151–2155.
123. Lao, K. U.; Schäffer, R.; Jansen, G. et al. Accurate Description of Intermolecular Interactions Involving Ions Using Symmetry-Adapted Perturbation Theory. *J. Chem. Theory Comput.* **2015,** *11*, 2473–2486.
124. Donchev, A. G.; Taube, A. G.; Decolvenaere, E. et al. Quantum Chemical Benchmark Databases of Gold-Standard Dimer Interaction Energies. *Sci. Data* **2021,** *8*, 55.
125. Carter-Fenk, K.; Herbert, J. M. Appraisal of Dispersion Damping Functions for the Effective Fragment Potential Method. *Mol. Phys.* **2023,** *121*, e2055504.
126. Villot, C.; Lao, K. U. Electronic Structure Theory on Modeling Short-Range Noncovalent Interactions Between Amino Acids. *J. Chem. Phys.* **2023,** *158*, 094301.
127. Sedlak, R.; Janowski, T.; Pitoňák, M. et al. Accuracy of Quantum Chemical Methods for Large Noncovalent Complexes. *J. Chem. Theory Comput.* **2013,** *9*, 3364–3374.
128. Tkatchenko, A.; Alfe, D.; Kim, K. S. First-Principles Modeling of Non-Covalent Interactions in Supramolecular Systems: The Role of Many-Body Effects. *J. Chem. Theory Comput.* **2012,** *8*, 4317–4322.
129. Ambrosetti, A.; Alfè, D.; DiStasio, Jr., R. A. et al. Hard Numbers for Large Molecules: Toward Exact Energetics for Supramolecular Systems. *J. Phys. Chem. Lett.* **2014,** *5*, 849–855.
130. Al-Hamdani, Y. S.; Tkatchenko, A. Understanding Non-Covalent Interactions in Larger Molecular Complexes from First Principles. *J. Chem. Phys.* **2019,** *150*, 010901.
131. Al-Hamdani, Y. S.; Nagy, P. R.; Zen, A. et al. Interactions Between Large Molecules Pose a Puzzle for Reference Quantum Mechanical Methods. *Nat. Commun.* **2021,** *12*, 3927.
132. Ni, Z.; Guo, Y.; Neese, F. et al. Cluster-in-Molecule Local Correlation Method with an Accurate Distant Pair Correction for Large Systems. *J. Chem. Theory Comput.* **2021,** *17*, 756–766.
133. Ballesteros, F.; Dunivan, S.; Lao, K. U. Coupled Cluster Benchmarks of Large Noncovalent Complexes: The L7 Dataset as Well as DNA-Ellipticine and Buckycatcher-Fullerene. *J. Chem. Phys.* **2021,** *154*, 154104.
134. Villot, C.; Ballesteros, F.; Wang, D. et al. Coupled Cluster Benchmarking of Large Noncovalent Complexes in L7 and S12L as Well as the C_{60} Dimer, DNA–ellipticine, and HIV–indinavir. *J. Phys. Chem. A* **2022,** *126*, 4326–4341.
135. Wolk, A. B.; Leavitt, C. M.; Garand, E. et al. Cryogenic Ion Chemistry and Spectroscopy. *Acc. Chem. Res.* **2014,** *47*, 202–210.

136. Tsybizova, A.; Fritsche, L.; Gorbachev, V. et al. Cryogenic Ion Vibrational Predissociation (CIVP) Spectroscopy of a Gas-Phase Molecular Torsion Balance to Probe London Dispersion Forces in Large Molecules. *J. Chem. Phys.* **2019,** *151*, 234304.
137. Gorbachev, V.; Tsybizova, A.; Miloglyadova, L. et al. Increasing Complexity in a Conformer Space Step-by-Step: Weighing London Dispersion Against Cation–π Interactions. *J. Am. Chem. Soc.* **2022,** *144*, 9007–9022.
138. Tsybizova, A.; Fritsche, L.; Miloglyadova, L. et al. Cryogenic Ion Vibrational Predissociation (CIVP) Spectroscopy of Aryl Cobinamides in the Gas Phase: How Good Are the Calculations for Vitamin B_{12} Derivatives?*J. Am. Chem. Soc.* **2023,** *145*, 19561–19570.
139. Antony, J.; Sure, R.; Grimme, S. Using Dispersion-Corrected Density Functional Theory to Understand Supramolecular Binding Thermodynamics. *Chem. Commun.* **2015,** *51*, 1764–1774.
140. Sure, R.; Grimme, S. Comprehensive Benchmark of Association (Free) Energies of Realistic Host–guest Complexes. *J. Chem. Theory Comput.* **2015,** *11*, 3785–3801. Erratum: J. Chem. Theory Comput. 2015, 11, 5990.
141. Assaf, K. I.; Florea, M.; Antony, J. et al. HYDROPHOBE Challenge: A Joint Experimental and Computational Study on the Host–guest Binding of Hydrocarbons to Cucurbiturils, Allowing Explicit Evaluation of Guest Hydration Free-Energy Contributions. *J. Phys. Chem. B* **2017,** *121*, 11144–11162.
142. Carter-Fenk, K.; Lao, K. U.; Liu, K.-Y. et al. Accurate and Efficient *ab Initio* Calculations for Supramolecular Complexes: Symmetry-Adapted Perturbation Theory with Many-Body Dispersion. *J. Phys. Chem. Lett.* **2019,** *10*, 2706–2714.
143. Liu, K.-Y.; Carter-Fenk, K.; Herbert, J. M. Self-Consistent Charge Embedding at Very Low Cost, with Application to Symmetry-Adapted Perturbation Theory. *J. Chem. Phys.* **2019,** *151*, 031102.
144. Nickerson, C. J.; Bryenton, K. R.; Price, A. J. A. et al. Comparison of Density-Functional Theory Dispersion Corrections for the DES15K Database. *J. Phys. Chem. A* **2023,** *127*, 8712–8722.
145. Ángyán, J.; Dobson, J.; Jansen, G. et al. *London Dispersion Forces in Molecules, Solids and Nano-Structures: An Introduction to Physical Models and Computational Methods;* 1st ed.; Royal Society of Chemistry,: Croydon, 2020.
146. Klimeš, J.; Bowler, D. R.; Michaelides, A. Chemical Accuracy for the van der Waals Density Functional. *J. Phys.: Condens. Matt* **2010,** *22*, 022201.
147. Cooper, V. R. Van der Waals Density Functional: An Appropriate Exchange Functional. *Phys. Rev. B* **2010,** *81* 161104(R).
148. Wellendorff, J.; Lundgaard, K. T.; Møgelhøj, A. et al. Density Functionals for Surface Science: Exchange-Correlation Model Development with Bayesian Error Estimation. *Phys. Rev. B* **2012,** *85*, 235149.
149. Hamada, I. Van der Waals Density Functional Made Accurate. *Phys. Rev. B* **2014,** *89* 121103(R). Erratum: Phys. Rev. B 2015, 91, 119902.
150. Berland, K.; Hylgaard, P. Exchange Functional That Tests the Robustness of the Plasmon Description of the van der Waals Density Functional. *Phys. Rev. B* **2014,** *89*, 035412.
151. Thonhauser, T.; Zuluaga, S.; Arter, C. A. et al. Spin Signature of Nonlocal Correlation Binding in Metal-Organic Frameworks. *Phys. Rev. Lett.* **2015,** *115*, 136402.
152. Peng, Q.; Wang, G.; Liu, G.-R. et al. Van der Waals Density Functional Theory vdW-DFq for Semihard Materials. *Crystals* **2019,** *9*, 243.
153. Thonhauser, T.; Cooper, V. R.; Li, S. et al. Van der Waals Density Functional: Self-Consistent Potential and the Nature of the van der Waals Bond. *Phys. Rev. B* **2007,** *76*, 125112.

154. Vydrov, O. A.; Wu, Q.; Van Voorhis, T. Self-Consistent Implementation of a Nonlocal van der Waals Density Functional with a Gaussian Basis Set. *J. Chem. Phys.* **2008,** *129*, 014106.
155. Gulans, A.; Puska, M. J.; Nieminen, R. M. Linear-Scaling Self-Consistent Implementation of the van der Waals Density Functional. *Phys. Rev. B* **2009,** *79* 201105(R).
156. Sabatini, R.; Gorni, T.; de Gironcoli, S. Nonlocal van der Waals Density Functional Made Simple and Efficient. *Phys. Rev. B* **2013,** *87* 041108(R).
157. Peng, H.; Yang, Z.-H.; Perdew, J. P. et al. Versatile van der Waals Density Functional Based on a Meta-Generalized Gradient Approximation. *Phys. Rev. X* **2016,** *6*, 041005.
158. Peng, H.; Perdew, J. P. Rehabilitation of the Perdew-Burke-Ernzerhof Generalized Gradient Approximation for Layered Materials. *Phys. Rev. B* **2017,** *95* 081105(R).
159. Terentjev, A. V.; Constantin, L. A.; Pitarke, J. M. Dispersion-Corrected PBEsol Exchange-Correlation Functional. *Phys. Rev. B* **2018,** *98*, 214108.
160. Terentjev, A. V.; Cortona, P.; Constantin, L. A. et al. Solid-State Testing of a van-der-Waals-Corrected Exchange-Correlation Functional Based on Semiclassical Atom Theory. *Computation* **2018,** *6*, 7.
161. Becke, A. D. Density-Functional Thermochemistry. V. Systematic Optimization of Exchange-Correlation Functionals. *J. Chem. Phys.* **1997,** *107*, 8554–8560.
162. Zhao, Y.; Truhlar, D. G. Density Functionals with Broad Applicability in Chemistry. *Acc. Chem. Res.* **2008,** *41*, 157–167.
163. Zhao, Y.; Truhlar, D. G. Applications and Validations of the Minnesota Density Functionals. *Chem. Phys. Lett.* **2011,** *502*, 1–13.
164. Peverati, R.; Truhlar, D. G. Quest for a Universal Density Functional: The Accuracy of Density Functionals Across a Broad Spectrum of Databases in Chemistry and Physics. *Phil. Trans. R. Soc. A* **2014,** *372*, 20120476.
165. Zhao, Y.; Schultz, N. E.; Truhlar, D. G. Design of Density Functionals by Combining the Method of Constraint Satisfaction with Parameterization for Thermochemistry, Thermochemical Kinetics, and Noncovalent Interactions. *J. Chem. Theory Comput.* **2006,** *2*, 364–382.
166. Perdew, J. P.; Constantin, L. A. Laplacian-Level Density Functionals for the Kinetic Energy Density and Exchange-Correlation Energy. *Phys. Rev. B* **2007,** *75*, 155109.
167. Staroverov, V. N.; Scuseria, G. E.; Tao, J. et al. Comparative Assessment of a New Nonempirical Density Functional: Molecules and Hydrogen-Bonded Complexes. *J. Chem. Phys.* **2003,** *119*, 12129–12137. Erratum: J. Chem. Phys. 2004, 121, 111507.
168. Goerigk, L.; Grimme, S. Double-Hybrid Density Functionals. *Wiley Interdiscip. Rev.: Comput. Mol. Sci.* **2014,** *4*, 576–600.
169. Brémond, E.; Ciofini, I.; Sancho-García, J. C. et al. Nonempirical Double-Hybrid Functionals: An Effective Tool for Chemists. *Acc. Chem. Res.* **2016,** *49*, 1503–1513.
170. Martin, J. M. L.; Santra, G. Empirical Double-Hybrid Density Functional Theory: A 'Third Way' in Between WFT and DFT. *Isr. J. Chem.* **2020,** *60*, 787–804.
171. Sancho-García, J.-C.; Brémond, E.; Pérez-Jiménez, A.-J. et al. Non-Empirical Quadratic-Integrand Double-Hybrid (QIDH) Functionals.*Annu. Rep. Comput. Chem.* **2023,** *19*, 87–119.
172. Nguyen, B.; Chen, G. P.; Agee, M. M. et al. Divergence of Many-Body Perturbation Theory for Noncovalent Interactions of Large Molecules. *J. Chem. Theory Comput.* **2020,** *16*, 2258–2273.
173. Calbo, J.; Ortí, E.; Sancho-García, J. C. et al. Accurate Treatment of Large Supramolecular Complexes by Double-Hybrid Density Functionals Coupled with Nonlocal van der Waals Corrections. *J. Chem. Theory Comput.* **2015,** *11*, 932–939.

174. Roch, L. M.; Baldridge, K. K. Dispersion-Corrected Spin-Component-Scaled Double-Hybrid Density Functional Theory: Implementation and Performance for Non-Covalent Interactions. *J. Chem. Theory Comput.* **2017,** *13*, 2650–2666.
175. Najibi, A.; Goerigk, L. A Comprehensive Assessment of the Effectiveness of Orbital Optimization in Double-Hybrid Density Functionals in the Treatment of Thermochemistry, Kinetics, and Noncovalent Interactions. *J. Phys. Chem. A* **2018,** *122*, 5610–5624.
176. Brémond, E.; Li, H.; Sancho-García, J. C. et al. Double Hybrids and Noncovalent Interactions: How Far Can We Go?*J. Phys. Chem. A* **2022,** *126*, 2590–2599.
177. Johnson, E. R.; Keinan, S.; Mori-Sánchez, P. et al. Revealing Noncovalent Interactions. *J. Am. Chem. Soc.* **2010,** *132*, 6498–6506.
178. Contreras-García, J.; Johnson, E. R.; Keinan, S. et al. NCIPLOT: A Program for Plotting Noncovalent Interaction Regions. *J. Chem. Theory Comput.* **2011,** 7, 625–632.
179. Narth, C.; Maroun, Z.; Boto, R. A. et al. A Complete NCI Perspective: From New Bonds to Reactivity. In *Applications of Topological Methods in Molecular Chemistry, Vol. 22;* Chauvin, R., Lepetit, C., Silvi, B., Eds.; Springer: Switzerland, 2016; pp. 491–527. Chapter 18.
180. Johnson, E. R.; Becke, A. D.; Sherrill, C. D. et al. Oscillations in Meta-Generalized-Gradient Approximation Potential Energy Surfaces for Dispersion-Bound Complexes. *J. Chem. Phys.* **2009,** *131*, 034111.
181. Johnson, E. R.; Mackie, I. D.; DiLabio, G. A. Dispersion Interactions in Density-Functional Theory. *J. Phys. Org. Chem.* **2009,** *22*, 1127–1135.
182. Wheeler, S. E.; Houk, K. N. Integration Grid Errors for Meta-GGA-Predicted Reaction Energies: Origin of Grid Errors for the M06 Suite of Functionals. *J. Chem. Theory Comput.* **2010,** *6*, 395–404.
183. Dasgupta, S.; Herbert, J. M. Standard Grids for High-Precision Integration of Modern Density Functionals: SG-2 and SG-3. *J. Comput. Chem.* **2017,** *38*, 869–882.
184. Morgante, P.; Peverati, R. The Devil in the Details: A Tutorial Review on Some Undervalued Aspects of Density Functional Theory Calculations. *Int. J. Quantum Chem.* **2020,** *120*, e26332.
185. Mardirossian, N.; Head-Gordon, M. Characterizing and Understanding the Remarkably Slow Basis Set Convergence of Several Minnesota Density Functionals for Intermolecular Interaction Energies. *J. Chem. Theory Comput.* **2013,** *9*, 4453–4461.
186. Goerigk, L. Testing London-Dispersion Effects with the Latest Minnesota Density Functionals: Problems and Possible Solutions. *J. Phys. Chem. Lett.* **2015,** *6*, 3891–3896.
187. Bircher, M. P.; López-Tarifa, P.; Rothlisberger, U. Shedding Light on the Basis Set Dependence of the Minnesota Functionals: Differences Between Plane Waves, Slater Functions and Gaussians. *J. Chem. Theory Comput.* **2019,** *15*, 557–571.
188. Jana, S.; Herbert, J. M. Fractional-Electron and Transition-Potential Methods for Core-to-Valence Excitation Energies Using Density Functional Theory. *J. Chem. Theory Comput.* **2023,** *19*, 4100–4113. Erratum: J. Chem. Theory Comput. 2023, 19, 7432–7433.
189. Furness, J. W.; Kaplan, A. D.; Ning, J. et al. Accurate and Numerically Efficient r^2SCAN Meta-Generalized Gradient Approximation. *J. Phys. Chem. Lett.* **2020,** *11*, 8208–8215. Erratum: J. Phys. Chem. Lett. 2020, 11, 9248.
190. Adamo, C.; Barone, V. Toward Reliable Density Functional Methods Without Adjustable Parameters: The PBE0 Model. *J. Chem. Phys.* **1999,** *110*, 6158–6170.
191. Sun, J.; Ruzsinszky, A.; Perdew, J. P. Strongly Constrained and Appropriately Normed Semilocal Density Functional. *Phys. Rev. Lett.* **2015,** *115*, 036402.
192. Grimme, S.; Ehrlich, S.; Goerigk, L. Effect of the Damping Function in Dispersion Corrected Density Functional Theory. *J. Comput. Chem.* **2011,** *32*, 1456–1465.

193. Smith, D. G. A.; Burns, L. A.; Patkowski, K. et al. Revised Damping Parameters for the D3 Dispersion Correction to Density Functional Theory. *J. Phys. Chem. Lett.* **2016,** *7*, 2197–2203.
194. Witte, J.; Mardirossian, N.; Neaton, J. B. et al. Assessing DFT-D3 Damping Functions Across Widely Used Density Functionals: Can We Do Better?*J. Chem. Theory Comput.* **2017,** *13*, 2043–2062.
195. Longuet-Higgins, H. C. Intermolecular Forces. *Discuss. Faraday Soc* **1965,** *40*, 7–18.
196. Herbert, J. M. Dielectric Continuum Methods for Quantum Chemistry. *Wiley Interdiscip. Rev.:Comput. Mol. Sci* **2021,** *11*, e1519.
197. Starkschall, G.; Gordon, R. G. Calculation of Coefficients in the Power Series Expansion of the Long-Range Dispersion Force Between Atoms. *J. Chem. Phys.* **1972,** *56*, 2801–2806.
198. Otero-de-la-Roza, A.; Johnson, E. R. Many-Body Dispersion Interactions from the Exchange-Hole Dipole Moment Model. *J. Chem. Phys.* **2013,** *138*, 054103.
199. Brinck, T.; Murray, J. S.; Politzer, P. Polarizability and Volume. *J. Chem. Phys.* **1993,** *98*, 4305–4306.
200. Fedorov, D. V.; Sadhukhan, M.; Stöhr, M. et al. Quantum-Mechanical Relation Between Atomic Dipole Polarizability and the van der Waals Radius. *Phys. Rev. Lett.* **2018,** *121*, 183401.
201. Tkatchenko, A.; Fedorov, D. V; Gori, M. Fine-Structure Constant Connects Electronic Polarizability and Geometric van-der-Waals Radius of Atoms. *J. Phys. Chem. Lett.* **2021,** *12*, 9488–9492.
202. e Proft, F., d; Vivas-Reyes, R.; Peeters, A. et al. Hirshfeld Partitioning of the Electron Density: Atomic Dipoles and Their Relation with Functional Group Properties. *J. Comput. Chem.* **2003,** *24*, 463–469.
203. Krishtal, A.; Senet, P.; Yan, M. et al. A Hirshfeld Partitioning of Polarizabilities of Water Clusters. *J. Chem. Phys.* **2006,** *125*, 034312.
204. Olasz, A.; Vanommeslaeghe, K.; Krishtal, A. et al. The Use of Atomic Intrinsic Polarizabilities in the Evaluation of the Dispersion Energy. *J. Chem. Phys.* **2007,** *127*, 224105.
205. Hirshfeld, F. L. Bonded-Atom Fragments for Describing Molecular Charge Densities. *Theor. Chem. Acc.* **1977,** *44*, 129–138.
206. Davidson, E. R.; Chakravorty, S. A Test of the Hirshfeld Definition of Atomic Charges and Moments. *Theor. Chem. Acc.* **1992,** *83*, 319–330.
207. Marenich, A. V.; Jerome, S. V.; Cramer, C. J. et al. Charge Model 5: An Extension of Hirshfeld Population Analysis for the Accurate Description of Molecular Interactions in Gaseous and Condensed Phases. *J. Chem. Theory Comput.* **2012,** *8*, 527–541.
208. Saha, S.; Roy, R. K.; Ayers, P. W. Are the Hirshfeld and Mulliken Population Analysis Schemes Consistent with Chemical Intuition?*Int. J. Quantum Chem.* **2009,** *109*, 1790–1806.
209. Heidar-Zadeh, F.; Ayers, P. W.; Verstraelen, T. et al. Information-Theoretic Approaches to Atoms-in-Molecules: Hirshfeld Family of Partitioning Schemes. *J. Phys. Chem. A* **2018,** *122*, 4219–4245.
210. Ángyán, J. G. On the Exchange-Hole Model of London Dispersion Forces. *J. Chem. Phys.* **2007,** *127*, 024108.
211. Otero-de-la-Roza, A.; Johnson, E. R. Non-Covalent Interactions and Thermochemistry Using XDM-Corrected Hybrid and Range-Separated Hybrid Density Functionals. *J. Chem. Phys.* **2013,** *138*, 204109.
212. Chu, X.; Dalgarno, A. Linear Response Time-Dependent Density Functional Theory for van der Waals Coefficients. *J. Chem. Phys.* **2004,** *121*, 4083–4088.
213. Tang, K. T. Dynamic Polarizabilities and van der Waals Coefficients. *Phys. Rev.* **1969,** *177*, 108–114.

214. Unsöld, A. Quantentheorie des Wasserstoffmolekülions und der Born-Landéschen Abstoßungskräfte. *Z. Phys* **1927,** *43*, 563–574.
215. Dalgarno, A.; Lewis, J. T. The Exact Calculation of Long-Range Forces Between Atoms by Perturbation Theory. *Proc. R. Soc. Lond. A* **1955,** *233*, 70–74.
216. Fukui, K.; Yamabe, T. A Note on the Theory of Interatomic Long-Range Forces. *Int. J. Quantum Chem.* **1968,** *2*, 359–369.
217. Mulder, F.; van Hemert, M.; Wormer, P. E. S. et al. *Ab Initio* Studies of Long Range Interactions Between Ethylene Molecules in the Multipole Expansion. *Theor. Chem. Acc.* **1977,** *46*, 39–62.
218. Sylvain, M. G.; Csizmadia, I. G. Average Dipole Polarizabilities from the Unsöld Approximation and *ab Initio* Data. *Chem. Phys. Lett.* **1987,** *136*, 575–582.
219. Ferri, N.; DiStasio, Jr., R. A.; Ambrosetti, A. et al. Electronic Properties of Molecules and Surfaces with a Self-Consistent Interatomic van der Waals Density Functional. *Phys. Rev. Lett.* **2015,** *114*, 176802.
220. DiStasio, Jr., R. A.; von Lilienfeld, O. A.; Tkatchenko, A. Collective Many-Body van der Waals Interactions in Molecular Systems. *Proc. Natl. Acad. Sci. USA* **2012,** *109*, 14791–14795.
221. Tkatchenko, A. Current Understanding of van der Waals Effects in Realistic Materials. *Adv. Funct. Mater.* **2015,** *25*, 2054–2061.
222. Reilly, A. M.; Tkatchenko, A. Van der Waals Dispersion Interactions in Molecular Materials: Beyond Pairwise Additivity. *Chem. Sci* **2015,** *6*, 3289–3301.
223. Ambrosetti, A.; Ferri, N.; DiStasio, Jr., R. A. et al. Wavelike Charge Density Fluctuations and van der Waals Interactions at the Nanoscale. *Science* **2016,** *351*, 1171–1176.
224. Hermann, J.; Alfè, D.; Tkatchenko, A. Nanoscale π–π Stacked Molecules Are Bound by Collective Charge Fluctuations. *Nat. Commun.* **2017,** *8*, 14052.
225. Dobson, J. F.; White, A.; Rubio, A. Asymptotics of the Dispersion Interaction: Analytic Benchmarks for van der Waals Energy Functionals. *Phys. Rev. Lett.* **2006,** *96*, 073201.
226. Gobre, V. V.; Tkatchenko, A. Scaling Laws for van der Waals Interactions in Nanostructured Materials. *Nat. Commun.* **2013,** *4*, 2341.
227. Dobson, J. F.; Gould, T.; Vignale, G. How Many-Body Effects Modify the van der Waals Interaction Between Graphene Sheets. *Phys. Rev. X* **2014,** *4*, 021040.
228. Ren, P.; Wu, C.; Ponder, J. W. Polarizable Atomic Multipole-Based Molecular Mechanics for Organic Molecules. *J. Chem. Theory Comput.* **2011,** 7, 3143–3161.
229. Shi, Y.; Xia, Z.; Zhang, J. et al. Polarizable Atomic Multipole-Based AMOEBA Force Field for Proteins. *J. Chem. Theory Comput.* **2013,** *9*, 4046–4063.
230. Zhang, C.; Lu, C.; Jing, Z. et al. AMOEBA Polarizable Atomic Multipole Force Field for Nucleic Acids. *J. Chem. Theory Comput.* **2018,** *14*, 2084–2108.
231. Jones, A. P.; Crain, J.; Sokhan, V. P. et al. Quantum Drude Oscillator Model of Atoms and Molecules: Many-Body Polarization and Dispersion Interactions for Atomistic Simulation. *Phys. Rev. B* **2013,** *87*, 144103.
232. Thole, B. T. Molecular Polarizabilities Calculated with a Modified Dipole Interaction. *Chem. Phys.* **1981,** *59*, 341–350.
233. Rappoport, D.; Furche, F. Property-Optimized Gaussian Basis Sets for Molecular Response Calculations. *J. Chem. Phys.* **2010,** *133*, 134105.
234. Kendall, R. A.; Dunning, Jr., T. H.; Harrison, R. J. Electron Affinities of the First-Row Atoms Revisited. Systematic Basis Sets and Wave Functions. *J. Chem. Phys* **1992,** *96*, 6796–6806.
235. Otero-de-la-Roza, A.; Johnson, E. R. Non-Covalent Interactions and Thermochemistry Using XDM-Corrected Hybrid and Range-Separated Hybrid Density Functionals. *J. Chem. Phys.* **2013,** *138*, 204109.

236. Boys, S. F.; Bernardi, F. The Calculation of Small Molecular Interactions by the Differences of Separated Total Energies. Some Procedures with Reduced Errors. *Mol. Phys.* **1970,** *19*, 553–566.
237. Tschumper, G. S. Reliable Electronic Structure Computations for Weak Noncovalent Interactions in Clusters. In *Reviews in Computational Chemistry, Vol. 26;* Lipkowitz, K. B., Cundari, T. R., Eds.; Wiley-VCH: Hoboken, 2009; pp. 39–90. Chapter 2.
238. Witte, J.; Neaton, J. B.; Head-Gordon, M. Push It to the Limit: Characterizing the Convergence of Common Sequences of Basis Sets for Intermolecular Interactions as Described by Density Functional Theory. *J. Chem. Phys.* **2016,** *144*, 194306.
239. Gray, M.; Bowling, P. E.; Herbert, J. M. In Defense of (Certain) Pople-Type Basis Sets. *ChemRxiv* **2024.** https://doi.org/10.26434/chemrxiv-2024-jz473.
240. Ashraf, A.; Carter-Fenk, K.; Herbert, J. M. et al. Interaction of Graphene Quantum Dots with Oligothiophene: A Comprehensive Theoretical Study. *J. Phys. Chem. C* **2019,** *123*, 29556–29570.
241. Ashraf, A.; Herbert, J. M.; Muhammad, S. et al. Theoretical Approach to Evaluate the Gas-Sensing Performance of Graphene Nanoribbon/Oligothiophene Composites. *ACS Omega* **2022,** 7, 2260–2274.
242. Hancock, A. C.; Goerigk, L. Noncovalently Bound Excited-State Dimers: A Perspective on Current Time-Dependent Density Functional Theory Approaches Applied to Aromatic Excimer Models. *RSC Adv* **2023,** *13*, 35964–359984.
243. Ikabata, Y.; Nakai, H. Extension of Local Response Dispersion Method to Excited-State Calculations Based on Time-Dependent Density Functional Theory. *J. Chem. Phys.* **2012,** *137*, 124106.
244. Hapka, M.; Przybytek, M.; Pernal, K. Symmetry-Adapted Perturbation Theory Based on Multiconfigurational Wave Function Description of Monomers. *J. Chem. Theory Comput.* **2021,** *17*, 5538–5555.
245. Hapka, M.; Krzemińska, A.; Modrzejewski, M. et al. Efficient Calculation of the Dispersion Energy for Multireference Systems with Cholesky Decomposition: Application to Excited-State Interactions. *J. Phys. Chem. Lett.* **2023,** *14*, 6895–6903.
246. Hohenstein, E. G.; Sherrill, C. D. Wavefunction Methods for Noncovalent Interactions. *Wiley Interdiscip. Rev.: Comput. Mol. Sci* **2012,** *2*, 304–326.
247. Szalewicz, K. Symmetry-Adapted Perturbation Theory of Intermolecular Forces. *Wiley Interdiscip. Rev.: Comput. Mol. Sci.* **2012,** *2*, 254–272.
248. Jansen, G. Symmetry-Adapted Perturbation Theory Based on Density Functional Theory for Noncovalent Interactions. *Wiley Interdiscip. Rev.: Comput. Mol. Sci* **2014,** *4*, 127–144.
249. Patkowski, K. Recent Developments in Symmetry-Adapted Perturbation Theory. *Wiley Interdiscip. Rev.: Comput. Mol. Sci* **2020,** *10*, e1452.
250. Carter-Fenk, K.; Lao, K. U.; Herbert, J. M. Predicting and Understanding Non-Covalent Interactions Using Novel Forms of Symmetry-Adapted Perturbation Theory. *Acc. Chem. Res.* **2021,** *54*, 3679–3690.
251. Lao, K. U.; Herbert, J. M. Energy Decomposition Analysis with a Stable Charge-Transfer Term for Interpreting Intermolecular Interactions. *J. Chem. Theory Comput.* **2016,** *12*, 2569–2582.
252. Stone, A. J. Physical Basis of Intermolecular Interactions. In *Non-Covalent Interactions in Quantum Chemistry and Physics;* de la Roza, A. O., DiLabio, G. A., Eds.; Elsevier: Amsterdam, 2017; pp. 3–26. Chapter 1.
253. Herbert, J. M. Simple, and Wrong: Debunking Electrostatic Fallacies Regarding Noncovalent Interactions. *J. Phys. Chem. A* **2021,** *125*, 7125–7137.
254. Szalewicz, K.; Jeziorski, B. Physical Mechanisms of Intermolecular Interactions from Symmetry-Adapted Perturbation Theory. *J. Mol. Model.* **2022,** *28*, 273.

255. Flick, J. C.; Kosenkov, D.; Hohenstein, E. G. et al. Accurate Prediction of Noncovalent Interaction Energies with the Effective Fragment Potential Method: Comparison of Energy Components to Symmetry-Adapted Perturbation Theory for the S22 Test Set. *J. Chem. Theory Comput.* **2012,** *8*, 2835–2843. Erratum: J. Chem. Theory Comput. 10, 4759-4760 (2014).
256. Parker, T. M.; Burns, L. A.; Parrish, R M. et al. Levels of Symmetry Adapted Perturbation Theory (SAPT). I. Efficiency and Performance for Interaction Energies. *J. Chem. Phys.* **2014,** *140*, 094106.
257. Schriber, J.; Cheney, D.; Sherrill, C. D. Levels of Symmetry Adapted Perturbation Theory (SAPT). II. Convergence of Interaction Energy Components. *ChemRxiv* **2023.** https://doi.org/10.26434/chemrxiv-2023-ftt1v.
258. Gray, M.; Herbert, J. M. Simplified Tuning of Long-Range Corrected Density Functionals for Symmetry-Adapted Perturbation Theory. *J. Chem. Phys.* **2021,** *155*, 034103.
259. Hohenstein, E. G.; Sherrill, C. D. Density Fitting of Intramonomer Correlation Effects in Symmetry Adapted Perturbation Theory. *J. Chem. Phys.* **2010,** *133*, 014101.
260. Bukowski, R.; Podeszwa, R.; Szalewicz, K. Efficient Calculation of Coupled Kohn–Sham Dynamic Susceptibility Functions and Dispersion Energies with Density Fitting. *Chem. Phys. Lett.* **2005,** *414*, 111–116.
261. Podeszwa, R.; Cencek, W.; Szalewicz, K. Efficient Calculations of Dispersion Energies for Nanoscale Systems from Coupled Density Response Functions. *J. Chem. Theory Comput.* **2012,** *8*, 1963–1969.
262. Gray, M.; Herbert, J. M. Comprehensive Basis-Set Testing of Extended Symmetry-Adapted Perturbation Theory and Assessment of Mixed-Basis Combinations to Reduce Cost. *J. Chem. Theory Comput.* **2022,** *18*, 2308–2330.
263. Shahbaz, M.; Szalewicz, K. Do Semilocal Density-Functional Approximations Recover Dispersion Energies at Small Intermonomer Separations?*Phys. Rev. Lett.* **2018,** *121*, 113402.
264. Shahbaz, M.; Szalewicz, K. Evaluation of Methods for Obtaining Dispersion Energies Used in Density Functional Calculations of Intermolecular Interactions. *Theor. Chem. Acc.* **2019,** *138*, 25.
265. Stasyuk, O. A.; Sedlak,; Guerra, C. F. et al. Comparison of the DFT-SAPT and Canonical EDA Schemes for the Energy Decomposition of Various Types of Noncovalent Interactions. *J. Chem. Theory Comput.* **2018,** *14*, 3440–3450.
266. Pernal, K.; Podeszwa, R.; Patkowski, K. et al. Dispersionless Density Functional Theory. *Phys. Rev. Lett.* **2009,** *103*, 263201.
267. Heßelmann, A. Comparison of Intermolecular Interaction Energies from SAPT and DFT Including Empirical Dispersion Contributions. *J. Phys. Chem. A* **2011,** *115*, 11321–11330.
268. Schriber, J. B.; Sirianni, D. A.; Smith, D. G. A. et al. Optimized Damping Parameters for Empirical Dispersion Corrections to Symmetry-Adapted Perturbation Theory. *J. Chem. Phys.* **2021,** *154*, 234107.
269. Lao, K. U.; Herbert, J. M. Accurate Intermolecular Interactions at Dramatically Reduced Cost: XPol+SAPT with Empirical Dispersion. *J. Phys. Chem. Lett.* **2012,** *3*, 3241–3248.
270. Lao, K. U.; Herbert, J. M. An Improved Treatment of Empirical Dispersion and a Many-Body Energy Decomposition Scheme for the Explicit Polarization Plus Symmetry-Adapted Perturbation Theory (XSAPT) Method. *J. Chem. Phys.* **2013,** *139*, 034107. Erratum: J. Chem. Phys. 2014, 140, 119901.
271. Jacobson, L. D.; Richard, R. M.; Lao, K. U. et al. Efficient Monomer-Based Quantum Chemistry Methods for Molecular and Ionic Clusters.*Annu. Rep. Comput. Chem.* **2013,** *9*, 25–58.

272. Lao, K. U.; Herbert, J. M. Symmetry-Adapted Perturbation Theory with Kohn-Sham Orbitals Using Non-Empirically Tuned, Long-Range-Corrected Density Functionals. *J. Chem. Phys.* **2014,** *140*, 044108.
273. Lao, K. U.; Herbert, J. M. Accurate and Efficient Quantum Chemistry Calculations of Noncovalent Interactions in Many-Body Systems: The XSAPT Family of Methods. *J. Phys. Chem. A* **2015,** *119*, 235–253.
274. Phipps, M. J. S.; Fox, T.; Tautermann, C. S. et al. Energy Decomposition Analysis Approaches and Their Evaluation on Prototypical Protein–Drug Interaction Patterns. *Chem. Soc. Rev.* **2015,** *44*, 3177–3211.
275. Francisco, E.; Pendás, A. M. Energy Partition Analyses: Symmetry-Adapted Perturbation Theory and Other Techniques. In *Non-Covalent Interactions in Quantum Chemistry and Physics;* de la Roza, A. O., DiLabio, G. A., Eds.; Elsevier: Amsterdam, 2017; pp. 27–64. Chapter 2.
276. Zhao, L.; von Hopffgarden, M.; Andrada, D. M. et al. Energy Decomposition Analysis. *Wiley Interdiscip. Rev.: Comput. Mol. Sci* **2018,** *8*, e1345.
277. Naseem-Khan, S.; Gresh, N.; Misquitta, A. J. et al. Assessment of SAPT and Supermolecular EDA Approaches for the Development of Separable and Polarizable Force Fields. *J. Chem. Theory Comput.* **2021,** *17*, 2759–2774.
278. Xu, Y.; Zhang, S.; Wu, W. et al. Assessments of DFT-Based Energy Decomposition Analysis Methods for Intermolecular Interactions. *J. Chem. Phys.* **2023,** *158*, 124116.
279. Clark, T.; Politzer, P.; Murray, J. S. Correct Electrostatic Treatment of Noncovalent Interactions: The Importance of Polarization. *Wiley Interdiscip. Rev.: Comput. Mol. Sci* **2015,** *5*, 169–177.
280. Mao, Y.; Ge, Q; Horn, P. R. et al. On the Computational Characterization of Charge-Transfer Effects in Noncovalently Bound Molecular Complexes. *J. Chem. Theory Comput.* **2018,** *14*, 2401–2417.
281. Stone, A. J. Natural Bond Orbitals and the Nature of the Hydrogen Bond. *J. Phys. Chem. A* **2017,** *121*, 1531–1534.
282. Weinhold, F.; Glendening, E. D. Comment on "Natural Bond Orbitals and the Nature of the Hydrogen Bond". *J. Phys. Chem. A* **2018,** *122*, 724–732.
283. Stone, A. J.; Szalewicz, K. Reply to "Comment on 'Natural Bond Orbitals and the Nature of the Hydrogen Bond'". *J. Phys. Chem. A* **2018,** *122*, 733–736.
284. Andrés, J.; Ayers, P. W.; Boto, R. A. et al. Nine Questions on Energy Decomposition Analysis. *J. Comput. Chem.* **2019,** *40*, 2248–2283.
285. Andrada, D. M.; Foroutan-Nejad, C. Energy Components in Energy Decomposition Analysis (EDA) Are Path Functions; Why Does It Matter?*Phys. Chem. Chem. Phys.* **2020,** *22*, 22459–22464.
286. Poater, J.; Andrada, D. M.; Solà, M. et al. Path-Dependency of Energy Decomposition Analysis & the Elusive Nature of Bonding. *Phys. Chem. Chem. Phys.* **2022,** *24*, 2344–2348.
287. Clark, T. How Deeply Should We Analyze Non-Covalent Interactions?*J. Mol. Model.* **2023,** *29*, 66.
288. Horn, P. R.; Mao, Y.; Head-Gordon, M. Probing Non-Covalent Interactions with a Second Generation Energy Decomposition Analysis Using Absolutely Localized Molecular Orbitals. *Phys. Chem. Chem. Phys.* **2016,** *18*, 23067–23079.
289. Horn, P. R.; Mao, Y.; Head-Gordon, M. Defining the Contributions of Permanent Electrostatics, Pauli Repulsion, and Dispersion in Density Functional Theory Calculations of Intermolecular Interaction Energies. *J. Chem. Phys.* **2016,** *144*, 114107.
290. Mao, Y.; Loipersberger, M.; Horn, P. R. et al. From Intermolecular Interaction Energies to Observable Shifts to Component Contributions and Back Again: A Tale of Variational Energy Decomposition Analysis. *Annu. Rev. Phys. Chem.* **2021,** *72*, 641–666.

291. Ziegler, T.; Rauk, A. On the Calculation of Bonding Energies by the Hartree Fock Slater Method. I. The Transition State Method. *Theor. Chem. Acc.* **1977,** *46*, 1–10.
292. Bickelhaupt, F. M.; Baerends, E. J. Kohn-Sham Density Functional Theory: Predicting and Understanding Chemistry. In *Reviews in Computational Chemistry, vol.* 15; Lipkowitz, K. B., Boyd, D. B., Eds.; Wiley-VCH: New York, 2000; pp. 1-86 Chapter 1.
293. Langlet, J.; Bergès, J.; Reinhardt, P. Decomposition of Intermolecular Interactions: Comparison Between SAPT and Density-Functional Decompositions. *J. Mol. Struct. (Theochem)* **2004,** *685*, 43–56.
294. Clark, T.; Murray, J. S.; Politzer, P. A Perspective on Quantum Mechanics and Chemical Concepts in Describing Noncovalent Interactions. *Phys. Chem. Chem. Phys.* **2018,** *20*, 30076–30082.
295. R^ezác, J.; Hobza, P. Extrapolation and Scaling of the DFT-SAPT Interaction Energies Toward the Basis Set Limit. *J. Chem. Theory Comput.* **2011,** 7, 685–689.
296. Nagy, P. R.; Kállay, M. Optimization of the Linear-Scaling Local Natural Orbital CCSD(T) Method: Redundancy-Free Triples Correction Using Laplace Transform. *J. Chem. Phys.* **2017,** *146*, 214106.
297. Nagy, P. R.; Samu, G.; Kállay, M. Optimization of the Linear-Scaling Local Natural Orbital CCSD(T) Method: Improved Algorithm and Benchmark Applications. *J. Chem. Theory Comput.* **2018,** *14*, 4193–4215.
298. Nagy, P. R.; Kállay, M. Approaching the Basis Set Limit of CCSD(T) Energies for Large Molecules with Local Natural Orbital Coupled-Cluster Methods. *J. Chem. Theory Comput.* **2019,** *15*, 5275–5298.
299. Nagy, P. R.; Gyevi-Nagy, L.; Lörincz, B. D. et al. Pursuing the Basis Set Limit of CCSD(T) Non-Covalent Interaction Energies for Medium-Sized Complexes: Case Study on the S66 Compilation. *Mol. Phys.* **2022,** *121*, e2109526.
300. Liakos, D. G.; Sparta, M.; Kesharwani, M. K. et al. Exploring the Accuracy Limits of Local Pair Natural Orbital Coupled-Cluster Theory. *J. Chem. Theory Comput.* **2015,** *11*, 1525–1539.
301. Sorathia, K.; Tew, D. P. Basis Set Extrapolation in Pair Natural Orbital Theories. *J. Chem. Phys.* **2020,** *153*, 174112.
302. Altun, A.; Neese, F.; Bistoni, G. Extrapolation to the Limit of a Complete Pair Natural Orbital Space in Local Coupled-Cluster Calculations. *J. Chem. Theory Comput.* **2020,** *16*, 6142–6149.
303. Altun, A.; Ghosh, S.; Riplinger, C. et al. Addressing the System-Size Dependence of the Local Approximation Error in Coupled-Cluster Calculations. *J. Phys. Chem. A* **2021,** *125*, 9932–9939.
304. Gray, M., Herbert, J. M. Evaluating the Domain-Based Local Pair Natural Orbital (DLPNO) Approximation for Noncovalent Interactions in Sizable van der Waals Complexes. *ChemRxiv*, **2024**. https://doi.org/10.26434/chemrxiv-2024-9cvcx.
305. Sparta, M.; Neese, F. Chemical Applications Carried out by Local Pair Natural Orbital Based Coupled-Cluster Methods. *Chem. Soc. Rev.* **2014,** *43*, 5032–5041.
306. Guo, Y.; Riplinger, C.; Becker, U. et al. Communication: An Improved Linear Scaling Perturbative Triples Correction for the Domain Based Local Pair-Natural Orbital Based Singles and Doubles Coupled Cluster Method [DLPNO-CCSD(T)]. *J. Chem. Phys.* **2018,** *148*, 011101.
307. Guo, Y.; Riplinger, C.; Liakos, D. G. et al. Linear Scaling Perturbative Triples Correction Approximations for Open-Shell Domain-Based Local Pair Natural Orbital Coupled Cluster Singles and Doubles Theory [DLPNO-CCSD(T_0/T)]. *J. Chem. Phys.* **2020,** *152*, 024116.

308. Liakos, D. G.; Neese, F. Comprehensive Benchmark Results for the Domain Based Local Pair Natural Orbital Coupled Cluster Method (DLPNO-CCSD(T)) for Closed- and Open-Shell Systems. *J. Phys. Chem. A* **2020,** *124*, 90–100.
309. Chen, Z.; Li, Y.; Chen, E. et al. Crystal Structure at 1.9-Å Resolution of Human Immunodeficiency Virus (HIV) II Protease Complexed with L-735,524, an Orally Bioavailable Inhibitor of the HIV Proteases. *J. Biol. Chem.* **1994,** *269*, 26344–26348.
310. Stiborova, M.; Sejbal, J.; Borek-Dohalska, L. et al. The Anticancer Drug Ellipticine Forms Covalent DNA Adducts, Mediated by Human Cytochromes P450, Through Metabolism to 13-Hydroxyellipticine and Ellipticine N^2 -Oxide. *Cancer Res.* **2004,** *64*, 8374–8380.
311. Benali, A.; Shulenburger, L.; Romero, N. A et al. Application of Diffusion Monte Carlo To Materials Dominated by van der Waals Interactions. *J. Chem. Theory Comput.* **2014,** *10*, 3417–3422.
312. Ucisik, M. N.; Dashti, D. S.; Faver, J. C. et al. Pairwise Additivity of Energy Components in Protein-Ligand Binding: The HIV II Protease-Indinavir Case. *J. Chem. Phys.* **2011,** *135*, 085101.
313. Hohenstein, E. G.; Parrish, R. M.; Sherrill, C. D. et al. Large-Scale Symmetry-Adapted Perturbation Theory Computations via Density Fitting and Laplace Transformation Techniques: Investigating the Fundamental Forces of DNA-Intercalator Interactions. *J. Chem. Phys.* **2011,** *135*, 174107.
314. Sherrill, C. D. Energy Component Analysis of π Interactions. *Acc. Chem. Res.* **2013,** *46*, 1020–1028.
315. Kamieth, M.; Burkert, U.; Corbin, P. S. et al. Molecular Tweezers as Synthetic Receptors: Molecular Recognition of Electron-Deficient Aromatic Substrates by Chemically Bonded Stationary Phases. *Eur. J. Org. Chem.* **1999,** *1999*, 2741–2749.
316. Allot, C.; Adams, H.; Hunter, C. A. et al. Hydrogen-Bond Recognition of Cyclic Dipeptides in Water. *Chem. Commun.* **1998,** *1998*, 2449–2450.
317. Grimme, S.; Hujo, W.; Kirchner, B. Performance of Dispersion-Corrected Density Functional Theory for the Interactions in Ionic Liquids. *Phys. Chem. Chem. Phys.* **2012,** *14*, 4875–4883.
318. Rudberg, E.; Rubensson, E. H.; Sałek, P. Kohn–Sham Density Functional Theory Electronic Structure Calculations with Linearly Scaling Computational Time and Memory Usage. *J. Chem. Theory Comput.* **2011,** *7*, 340–350.
319. Rudberg, E. Difficulties in Applying Pure Kohn–Sham Density Functional Theory Electronic Structure Methods to Protein Molecules. *J. Phys.: Condens. Matt* **2012,** *24*, 072202.
320. Isborn, C. M.; Mar, B. D.; Curchod, B. F. E. et al. The Charge Transfer Problem in Density Functional Theory Calculations of Aqueously Solvated Molecules. *J. Phys. Chem. B* **2013,** *117*, 12189–12201.
321. Kulik, H. J.; Luehr, N.; Ufimtsev, I. S. et al. Ab *initio* Quantum Chemistry for Protein Structures. *J. Phys. Chem. B* **2012,** *116*, 12501–12509.
322. Lever, G.; Cole, J. D.; Hine, N. D. M. et al. Electrostatic Considerations Affecting the Calculated HOMO-LUMO Gap in Protein Molecules. *J. Phys.: Condens. Matt* **2013,** *25*, 152101.
323. Antony, J.; Grimme, S. Fully *ab Initio* Protein-Ligand Interaction Energies with Dispersion Corrected Density Functional Theory. *J. Comput. Chem.* **2012,** *33*, 1730–1739.
324. Cole, D. J.; Hine, N. D. M. Applications of Large-Scale Density Functional Theory in Biology. *J. Phys.: Condens. Matt* **2016,** *28*, 393001.
325. Ren, F.; Liu, F. Impacts of Polarizable Continuum Models on the SCF Convergence and DFT Delocalization Error of Large Molecules. *J. Chem. Phys.* **2022,** *157*, 184106.

326. Bowling, P. E.; Broderick, D. R.; Herbert, J. M. Fragment-Based Calculations of Enzymatic Thermochemistry Require Dielectric Boundary Conditions. *J. Phys. Chem. Lett.* **2023,** *14*, 3826–3834.
327. Lange, A.; Herbert, J. M. Simple Methods to Reduce Charge-Transfer Contamination in Time-Dependent Density-Functional Calculations of Clusters and Liquids. *J. Chem. Theory Comput.* **2007,** *3*, 1680–1690.
328. Slattery, S. A.; Surjuse, K. A.; Peterson, C. et al. Economical Quasi-Newton Unitary Optimization of Electronic Orbitals. *Phys. Chem. Chem. Phys.* **2024,** *26*, 6557–6573.
329. Summers, T. J.; Cheng, Q.; Palma, M. A. et al. Cheminformatic Quantum Mechanical Enzyme Model Design: A Catechol-O-Methyltransferase Case Study. *Biophys. J.* **2021,** *120*, 3577–3587.
330. Cheng, Q.; DeYonker, N. J. The Glycine N-Methyltransferase Case Study: Another Challenge for QM-Cluster Models? *J. Phys. Chem. B* **2023,** *127*, 9282–9294.
331. Agbaglo, D. A.; Summers, T. J.; Cheng, Q. et al. The Influence of Model Building Schemes and Molecular Dynamics on Qm-Cluster Models: The Chorismate Mutase Case Study. *ChemRxiv* **2024.** https://doi.org/10.26434/chemrxiv-2023-fvzp6-v2.
332. Enkvist, C.; Zhang, Y.; Yang, W. Density Functional Study of a Weakly Hydrogen-Bonded Benzene–ammonia Complex: The Importance of the Exchange Functional. *Int. J. Quantum Chem.* **2000,** *79*, 325–329.
333. Salazar, M. C.; Paz, J. L.; Hernández, A. J. et al. Density Functional Theory Test Study on the CO ⋯ He Dimer. *Int. J. Quantum Chem.* **2003,** *95*, 177–183.
334. Hansen, A.; Bannwarth, C.; Grimme, S. et al. The Thermochemistry of London Dispersion-Driven Transition Metal Reactions: Getting the 'Right Answer for the Right Reason'. *ChemistryOpen* **2014,** *3*, 177–189.
335. Verevkin, S. P.; Kondratev, S. O.; Zaitsau, D. H. et al. Quantification and Understanding of Non-Covalent Interactions in Molecular and Ionic Systems: Dispersion Interactions and Hydrogen Bonding Analysed by Thermodynamic Methods. *J. Mol. Liq.* **2021,** *343*, 117547.
336. Ohio Supercomputer Center 2024 (http://osc.edu/ark:/19495/f5s1ph73).
337. Epifanovsky, E.; Gilbert, A. T. B.; Feng, X. et al. Software for the Frontiers of Quantum Chemistry: An Overview of Developments in the Q-Chem 5 Package. *J. Chem. Phys.* **2021,** *155*, 084801.
338. Kong, J.; Gan, Z.; Proynov, E. et al. Efficient Computation of the Dispersion Interaction with Density-Functional Theory. *Phys. Rev. A* **2009,** *79*, 042510.